https://doi.org/10.1016/j.ymssp.2021.107847

Prediction Error of Johansen Cointegration Residuals for Structural Health Monitoring

Mohsen Mousavi[a], Amir H. Gandomi *[a]

[a]Faculty of Engineering and IT, University of Technology Sydney, Ultimo, NSW 2007, Australia

**Abstract**

A novel method for structural health monitoring under environmental and operational variations (EOV) is proposed based on the prediction errors of the Johansen cointegartion (CI) residuals using a Recurrent Neural Network (RNN). The first four natural frequency time series of the structure, identified from vibration measurements over a period of time, are used to this end. The Variational Mode Decomposition (VMD) algorithm is first used for denoising and removing seasonal patterns in the frequency signals. The first modes of the decomposition results corresponding to all frequency signals are then used to obtain Johansen CI residuals. Next, a portion of the obtained signals form VMD decomposition along with the same portion of the Johansen CI residuals are used respectively as training feature and targets to train a RNN. The trained RNN is then used to predict the future CI residuals from the remaining portion of the features. The error of the prediction results is used as damage sensitive feature. The proposed method has been successfully tested on both a long-term monitoring problem of a numerical example (spring-mass system), a short-term monitoring problem regarding an experimental example (wooden bridge), and a long-term monitoring of an experimental example (bridge Z24). The results demonstrate the capability of the proposed method in monitoring structures for damage even when the Johansen algorithm fails to identify a linear CI relationship among the frequency signals.

*Keywords:* Structural Health Monitoring, Environmental and Operational Variations, Johansen Cointegration, Variational Mode Decomposition, Recurrent Neural Netwrok

11

*Email address:* gandomi@uts.edu.au (Amir H. Gandomi *)

## 1. Introduction

The main trend in Structural Health Monitoring (SHM) over the past decades has been toward using two main strategies: (1) model based and (2) data based techniques. Model-based techniques basically seek to update damage parameters in a Finite Element (FE) model of the structure using some response measured on the real structure. As such, FE modeling is a common computational technique used to model complex structures for this purpose [1]. As such, different parameters corresponding to the FE model of the structure are updated through minimising an objective function constructed based on the difference between the computed and measured structural response [1]. Therefore, several runs, equal to the number of iterations for the optimisation problem to converge, of a computer algorithm are required to successfully update the structural parameters. While model-based techniques are relying on the physics of the problem, data based methods seek to find anomaly in structures based on pure mathematical principals governing the nature of the data.

It is known that operational and environmental variations (EOV) can affect the mode shape and natural frequencies of structures. These variations, which have non-stationary effects on signals, will bring about false-positive or false-negative outcomes in damage detection algorithms. It is known that temperature is the primary environmental influence on the structural modal properties and subsequently can mask the effect of damage in structural response [2]. It has been reported that there is a strong long-term correlation between variation of natural frequencies and temperature [3, 4]. For instance, the results of a study conducted on a two span steel-concrete composite bridge in North Carolina showed that the absolute variation of the measured first five natural frequencies of the bridge between the night and noon is roughly between 1 and 2 percent when the temperature during this period in the top of concrete, top flange, and the bottom flange varies 26.30, 18.95, 7.50 percent, respectively [5].

One remedy to deal with this problem is data normalisation [6]. Data normalisation can be regarded as a data fusion technique aiming at obtaining a stationary representation of a set of given non-stationary signals. This stationary representation does not include the EOV effects and, therefore, can be reliably used for monitoring structures. A property of a set of non-stationary time series where a linear combination of them can produce a stationary residual is referred to as cointegration (CI). These residuals can be further used as potentially effective damage features in damage detection algorithms [7]. As such, the parameters of this linear combination are usually referred to as a CI vector which can be identified using Johansen procedure [8] or Engle-Granger (EG) two-step procedure [9].

There are however, some challenges with using CI for SHM. It has been argued that while the measured responses from healthy structure show non-stationary behaviour in the short run (a couple of days), they have usually stationary trend over a long period of time (a couple of months) [10]. This fact will further undermine the basic unit root assumption of the signals for CI when using a fraction of the data as training set. However, it has been suggested that the philosophical question of whether a unit root assumption is valid can be overlooked from the engineering application point of view [10].

Dao et al. used CI to mitigate the effect of temperature variation in damage detection using lamb waves [11]. In another study, Dao et al. applied cointergartion to the non-linear vibro-acoustic modulation [12] waves from low frequency excitation of laminated composite plates and composite sandwich panels for removing the effect of variable operational conditions [13]. Li et al. used a Johansen test [14] to obtain the CI residuals of electro-mechanical impedance responses for removing temperature effects on damage detection [15]. Tomé et al. also used the multivariate CI analysis following the multivariate Johansen procedure to remove the operational and environmental effects on damage detection [16]. The CI interpretation of time series has been also used as a diagnostic measure for damage detection using recorded vibration signals [17]. One problem with using linear conintegration method arises from the *heteroscedasticity* nature of the time series [18] where the stationary assumption for the variance of the residual around the regression line is not valid. In contrast, *homoscedastic* cointegrated time series have strictly stationary residuals. The Breusch–Pagan test is usually used to determine the presence of heteroscedasticity in the CI residuals either in linear or non-linear CI [18].

There are two types of CI algorithms, namely linear and nonlinear. As first attempts to formulate a non-linear CI method for SHM purposes, variants of the Johansen and EG procedures were used in an evolutionary optimisation framework to estimate parameters for multinomial cointegrating relationships [19, 20]. The problem occurred in these papers, was that the CI residuals obtained from the methods were heteroscedastic. To address this issue, it was proposed that the non-stationarity from the variance of the residual sequence be moved to its tail distribution [21]. Nevertheless, there was still a problem with the normal control chart thresholds not being appropriate [22]. Machine learning algorithms such as least-squares support vector machines [23], Relevance Vector Machines (RVMs) [24], Gaussian Process Regression (GPR) [22] have been used to deal with this problem. As such, a portion of the signals is used as a training set to find the underlying non-linear CI relationship. However, once the damage occurs, the underlying CI relationship may no longer hold, and consequently the CI residuals will no longer stay stationary [25, 24]. Although data normalisation has been proven to be able to detect damage at the presence of EOV, two major problems have been reported in the literature. These are: (1) dependency to large number of healthy training data under different environmental and operational conditions for creating the CI residuals, and (2) the CI relationship among variables cannot be determined in damage state. To overcome the two drawbacks, the Kalman Filter (KF) was used along with CI to online estimate the change of the CI relationship [26].

In this paper, a novel and effective method for monitoring of structures using recorded structural response under EOV is proposed. To that end, the identified frequency time series of the structure are decomposed into their two oscillatory modes using the Variational Mode Decomposition (VMD) algorithm [27]. The decomposed modes are: 1) a DC non-stationary signal which has 0 center frequency and contains information about the damage state of the structure, and 2) a stationary seasonal mode which is believed will interfere with damage detection. Therefore, only the non-stationary mode of the signals is used to construct Johansen CI residuals. Then a part of the obtained Johansen CI and the first mode of the frequency time series are used respectively as target and features to train a Recurrent Neural Network (RNN). The trained RNN is then used to predict the future CI relationship using remaining part of the first modes signals as test features. The results are compared against the corresponding obtained Johansen CI. It is shown that the prediction error will significantly deviate from the average value of the errors when a damage occurs in the system. The proposed strategy is tested successfully on both a long-term monitoring of a numerical example as well as a short-term and long-term monitoring of two different experimental examples.

There are four different phases regarding the SHM in general which are: 1) monitoring structures for any change due to damage, 2) locating the damage, 3) recognising the type of the damage, and 4) quantifying the severity of the damage [28]. The method of this paper falls into the first category where raising an early alarm is intended as soon as the structure undergoes any changes that can be referred to damage.

## 2. Cointegration

### 2.1. Stationary and non-stationary signals

The concept of CI has a deep connection with the notation of stationary and non-stationary definition of a time series [29]. Therefore, a brief definition of the stationary and non-stationary time series is presented in here [18, 11].

Consider the signal $X(t)$, the first order auto-regressive process $AR(1)$ of the signal is obtained as follows,

$$X(t) = \phi\, X(t-1) + \epsilon_t \tag{1}$$

Where $\epsilon_t$ is a stationary white Gaussian noise process. As such three cases can happen for the $AR(1)$ model of the time series $X(t)$ which are; 1) $|\phi| < 1$, where the signal is stationary, 2) $|\phi| > 1$, implies the signal is non-stationary, and 3) $|\phi| = 1$, that represents a pure random walk model which is also non-stationary due to the explosion of the variance as $t \to \infty$.

A time series is referred to as unit root process when its characteristic function has a unit root. In econometrics, when a deterministic trend is the cause of non-stationarity, the time series is referred to as trend stationary process. When the non-stationarity is due to the unit root, the time series is referred to as difference stationary process. This is mainly due to the fact that difference operation will render the series stationary. The best example is when this type of transformation is applied to a first order non-stationary pure random walk process $I(1)$ where $\Delta X(t) = X(t) - X(t-1) = \epsilon_t$ is a stationary white Gaussian noise process $I(0)$. The reasons for using CI instead of working simply with difference signals in SHM are as follows [10],

1. Numerical differentiation of experimental data will greatly amplify any high frequency noise components, whereas CI will at worst generate a weighted average of the noise.
2. Differentiation will remove any trend in the data associated with damage.

There are, however, other notions of the stationary and non-stationary signals. For instance, a stationary signal has time-invariant statistical moments whereas the moments of a non-stationary signal show some time dependence. A weak assumption for the stationary of a signal is obtained when only the first two statistical moments of the signal are time invariant.

### 2.2. Johansen cointegration

Cointegration (CI) is a technique adapted from the field of econometrics for removing trends induced by environmental and operational variations in measured data used for damage detection [8, 10]. The Johansen procedure can be used to not only estimate multiple CI vectors, but also to produce a test statistic for determining the number of CI vectors. It is said that a time series $X(t)$ is integrated of order $d$ if $\Delta^d X(t)$ is stationary where $\Delta X(t) = X(t) - X(t-1)$. Note that $\Delta^d$ indicates $d$ times application of the difference operator $\Delta$ to the signal $X(t)$. As such, $m$ signals $\{X_1(t), \ldots, X_m(t)\}$ are cointegrated with order $d$ and $b$ if two following conditions are satisfied,

1. Each signal $X_i(t)$, $i = 1, \ldots, m$, is integrated of order $d$. The Kwiatkowski–Phillips–Schmidt–Shin (KPSS) and Augmented Dickey-Fuller (ADF) tests are two main unit root tests to determine how many times the difference operator $\Delta$ should be applied to make the time series stationary.

2. There exists a linear combination of the signals $X_i(t)$ such as,

$$\Psi(t) = a_1\, X_1(t) + a_2\, X_2(t) + \cdots + a_m\, X_m(t) \tag{2}$$

so that $\Psi(t)$ is integrated of order $d-b$. In such a case, the time series $\{X_1(t), \ldots, X_m(t)\}$ are denoted as CI$(d, b)$. The most common case is when $d = b = 1$. The vector $[a_1, \ldots, a_m]$ is the CI vector and can be obtained using a least squares optimisation algorithm [30]).

Take $Y_t = \{X_1(t), \ldots, X_m(t)\}^T$ as a $m \times 1$ $I(1)$ vector where $m$ is the number of features measured on the structure at time $t$. These features are usually a couple of first natural frequencies of the structure. To perform Johansen procedure, a vector autoregressive (VAR) model of $Y_t$ is constructed as follows,

$$Y_t = \delta D_t + \sum_{j=1}^{p} \Phi_j Y_{t-j} + u_t \tag{3}$$

where $p$ is the lag order, $D_t$ denotes the vector of deterministic variables such as constant, trends, and/or seasonal dummy variables, and $\Phi_j$ and $u_t$ are respectively a $m \times m$ coefficient matrix and $m \times 1$ *iid* Gaussian noise vector. Substituting $Y_t = Y_{t-1} + \Delta Y_t$, $Y_{t-1} = Y_{t-2} + \Delta Y_{t-1}$, $\ldots$, $Y_{t-p} = Y_{t-p-1} + \Delta Y_{t-p}$ into (3) we get the error correction model (ECM) as follows,

$$\Delta Y_t = \Gamma_o D_t + \Pi Y_{t-1} + \sum_{j=1}^{p-1} \Gamma_j \Delta Y_{t-j} + u_t \tag{4}$$

where $\Pi = -(I - \Phi_1 - \ldots \Phi_p)$ and $\Gamma_j = -(\Phi_{j+1} + \ldots \Phi_p)$ for $j = 1, \ldots, p-1$. $\Pi Y_{t-1}$ is called error-correction term. There are three possibility for the $rank(\Pi) = r$ as can be seen in Table 1. As such, the Johansen CI relationship among $\{X_1, \ldots, X_m\}$ exist only when $0 < r < m$. In such a case, $\Pi$ is factorised as $\alpha\ \beta^T$ where $\alpha$ and $\beta$ are adjustment and CI matrices. Note that the aforementioned factorisation is not unique and, therefore, in order to get a unique factorisation as such, further restrictions need to be imposed. To that end, Johansen proposed a maximum likelihood method as follows.

Substituting $Z_{0t} = \Delta Y_t$, $Z_{1t} = Y_{t-1}$, $Z_{2t} = \{\Delta Y_{t-1}, \ldots, \Delta Y_{t-p-1}, D_t\}^T$, $\Psi = \{\Gamma_1, \ldots, \Gamma_p, \Gamma_0\}$, and $\Pi = \alpha\ \beta^T$ into (4) gives,

$$Z_{0t} = \alpha\ \beta^T Y_{t-1} + \Psi Z_{2t} + \epsilon_t \tag{5}$$

Assuming normality for $\epsilon_t \sim N(0, \Sigma)$, the logarithm likelihood function can be constructed as follows,

$$\begin{aligned} lnL(\alpha, \beta, \Sigma | Y_t) = -\tfrac{mN}{2} log(2\pi) - \tfrac{N}{2} log(|\Sigma|) \\ -\tfrac{1}{2} \textstyle\sum_{t=1}^{N} \left(Z_{0t} - \alpha\beta^T Z_{1t} - \Psi Z_{2t}\right)^T \Sigma^T \left(Z_{0t} - \alpha\beta^T Z_{1t} - \Psi Z_{2t}\right) \end{aligned} \tag{6}$$

Table 1: The model properties for different cases of $rank(\Pi) = r$.

| rank (Π)=r | Properties |
|---|---|
| r=0 | 1) All eigenvalues of Π are zero.<br>2) $\Pi = \mathbf{0}$.<br>3) $\{X_1, \ldots, X_m\}$ are not correlated. |
| r=m | 1) $\lvert\Pi\rvert \neq 0$.<br>2) $\{X_1, \ldots, X_m\}$ are of $I(0)$.<br>3) The relationship of $\{X_1, \ldots, X_m\}$ can be modeled in level and not in differences.<br>4) here is no need to refer to the error correction representation. |
| $0 < r < m$ | 1) each of $\{X_1, \ldots, X_m\}$ is integrated of $I(1)$.<br>2) Π has $r$ nonzero eigenvalues.<br>3) All $\{X_1, \ldots, X_m\}$ are cointegrated and there is $r$ CI relationships. |

where $N$ is the number of observations. In order to estimate the unknown parameters, i.e. $\alpha$ and $\beta$, in maximum likelihood problem of (6), residuals $R_{0t}$ and $R_{1t}$ are obtained by regressing $Z_{0t}$ and $Z_{1t}$ on $Z_{2t}$, respectively. Therefore, the VECM of (4) can be written as,

$$S_{ij} = \frac{1}{N} \sum_{t=1}^{N} R_{it} R_{jt} \tag{7}$$

Obtaining $\alpha$ and $\beta$ requires solving the following eigenvalue problem,

$$\left| \lambda_i S_{11} - S_{10} S_{00}^{-1} S_{01} \right| = 0 \tag{8}$$

Assuming that $\{\lambda_1, \ldots, \lambda_r\}$ are $r$ eigenvalues of (8), the corresponding eigenvectors $\{v_1, \ldots, v_r\}$ construct the cointegrating matrix $\beta$ as follows,

$$\hat{\beta} = \beta_{MLE} = [v_1, \ldots, v_r] \tag{9}$$

The eigenvector corresponding to the largest eigenvalue represents the first CI vector which is the “most stationary” CI vector as well [30]. MATLAB Econometric Toolbox is used in this paper to obtain the eigenvectors corresponding to the first two largest eigenvalues obtained from the Johansen procedure.

## 3. Proposed damage detection strategy

Diagram of Figure 1 shows the routine procedure followed for obtaining CI relationships among a set of input signals. In theory, the Johansen procedure is said to be successful when the

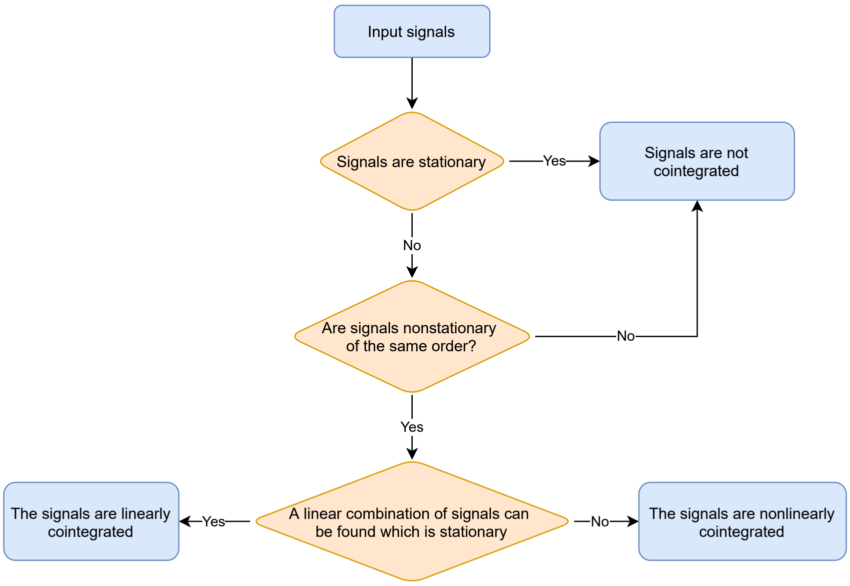


Figure 1: Diagram of examining signals for linear or non-linear CI.

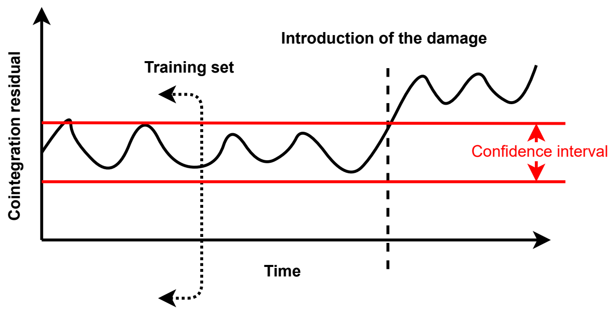


Figure 2: Damage detection using trained non-linear CI residuals.

resulted residuals from a set of $I(1)$ inputs is stationary ($I(0)$). When the Johansen procedure is not successful a non-linear CI procedure can be devised. In SHM, machine learning algorithms have been used to this end. As such, a portion of the input signals is used as a training set to train a non-linear CI relationship among them (Figure 2). When the damage happens, the underlying CI relationship does not hold any longer and an alarm is raised. In this section, first a strategy based on the prediction of Johansen CI using a RNN is outlined. Then, a numerical example is presented to walk the readers through the proposed structural condition monitoring method in the next section.

Conventional damage detection algorithms suffer from the change of the variance of heteroscedastic data which makes the procedure of damage detection more complex. Therefore, the first step is to remove any complex seasonal patterns in the applied signals prior to cointegration analysis [25]. To that end, VMD is used in this paper for both denoising and removing the seasonal patterns in the signals. VMD is a parametric decomposition algorithm and thus cares need to be taken when specifying its parameters. The theory of the VMD and ways of choosing

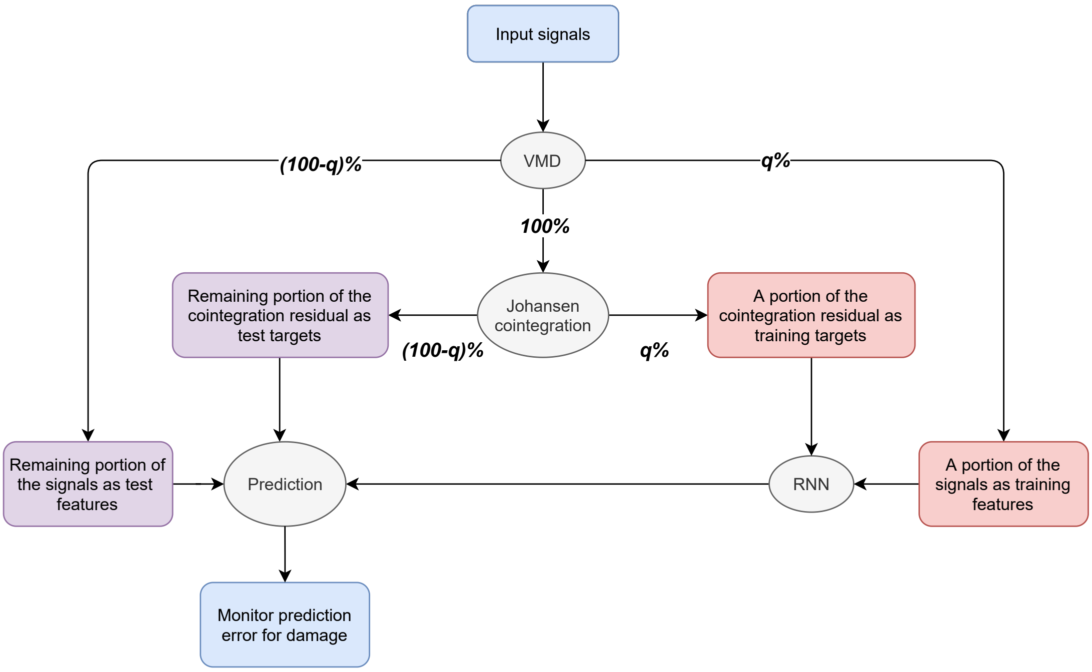


Figure 3: The diagram of the proposed damage detection method.

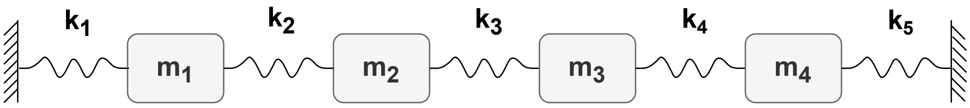


Figure 4: A four degree of freedom spring-mass system.

its parameters will be discussed in a following section.

Next step is to use 100% of the VMD outcomes to construct CI residuals. Then, $q\%$ of the VMD outcomes along with $q\%$ of the Johansen CI residuals corresponding to the healthy structure are used respectively as features and targets to train a recurrent neural network (RNN). This is done in order to learn the underling Johansen CI relationship related to the healthy structure in an alternative way. The last step is to use the trained RNN to predict the future CI relationship using $(100 - q)\%$ of the VMD outcome as the test features. The results of the prediction is then compared against the remaining $((100-q)\%)$ part of the Johansen CI residuals. It will be shown that the error in the prediction will significantly deviate from the average error when damage occurs. The procedure of the proposed strategy is shown in the diagram of Figure 3.

## 4. Illustrative numerical example

A four degree of freedom (DOF) spring-mass system is presented in this section as an illustrative example (Figure 4). The example is similar to the one used in [30] with some adjustments. As such, the weight of the masses is equal to 2 $kg$ each. The stiffness of each spring is in $kN/m$

https://doi.org/10.1016/j.ymssp.2021.107847

and is assumed to vary with temperature as follows,

$$k_i = \begin{cases} -0.11 \times T + 4, & \text{if } T < 0 \\ -0.03 \times T + 4, & \text{if } T \geq 0 \end{cases} \tag{10}$$

for $i = 1, 2, 4, 5$, and

$$k_3 = \begin{cases} -0.11 \times T + 5, & \text{if } T < 0 \\ -0.2 \times T + 5, & \text{if } T \geq 0 \end{cases} \tag{11}$$

The different behaviour of $k_3$ has non-linear effect on vibration modes. A -15 $^oC$ shifted[1] 10000 temperature records of Basel-Switzerland is used in this section (Figure 5a) [31]. The temperatures are recorded hourly and the time period of the records is from June 2019 to July 2020. It is assumed that the stiffness of $k_3$ reduces by 20% at $7000^{th}$ record and this reduction of stiffness lasts for the duration of 100 records. As such, we assume that the damage is detected and then fixed afterwards. The four natural frequencies of the system are calculated at each time instant and 10% noise is added to the signals using the following equation [32],

$$\hat{\delta} = \delta + \frac{\kappa}{100} n_{\text{noise}}\ \sigma(\delta), \tag{12}$$

where $\delta$ and $\hat{\delta}$ represent respectively the vector of noise-free and noisy calculated frequencies. $\sigma(\delta)$ represents the standard deviation of $\delta$ and $\kappa$ is the noise level (= 10). $n_{\text{noise}}$ is a random independent variables vector of the same length as $\delta$ following a standard normal distribution. Figure 5b shows the obtained four noisy natural frequency time series of the spring-mass system. Next, we exploit VMD for denoising and removing the seasonal patterns in the frequency signals. Since VMD is a parametric signal decomposition algorithm, ways of specifying its parameters are discussed in the following section.

### *4.1. Variational Mode Decomposition (VMD)*

VMD is an advanced signal decomposition algorithm which is able to decompose a non-linear non-stationary signal into $k$ oscillatory modes known as Intrinsic Mode Functions (IMF). The sum of which can construct the noisefree original signal depending on settings [33]. Each IMF is narrow-band and has a center frequency $\omega$. VMD solves the following optimisation problem,

$$\min_{\{u_k\}\ \&\ \{\omega_k\}} \sum_k \left\| \partial_t \left( \delta(t) + \frac{j}{\pi t} * u_k(t) \right) e^{-j\omega_k t} \right\|^2 \tag{13}$$

where $*$ and $j$ are respectively the convolution operator and the imaginary unit. Quoted from the proposers of VMD, the solution to the above minimisation problem is the saddle point of

[1]The reason for shifting temperatures -15 $^oC$ is to provide a wide of range of negative and positive temperature profile.

https://doi.org/10.1016/j.ymssp.2021.107847

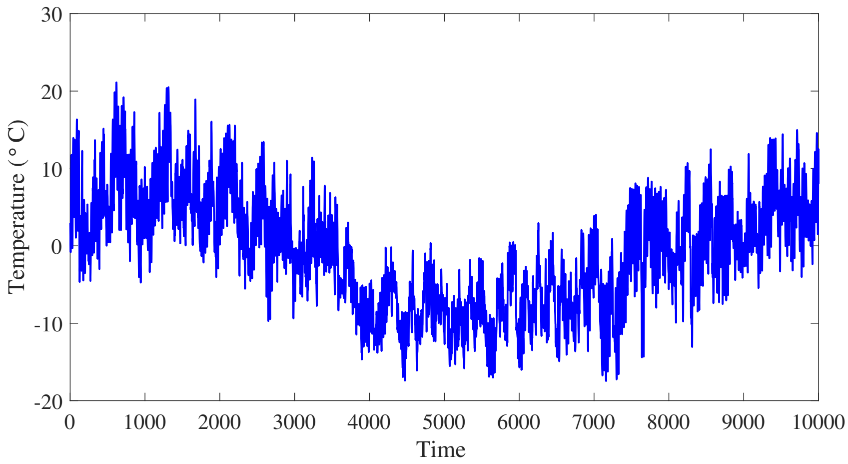


(a)

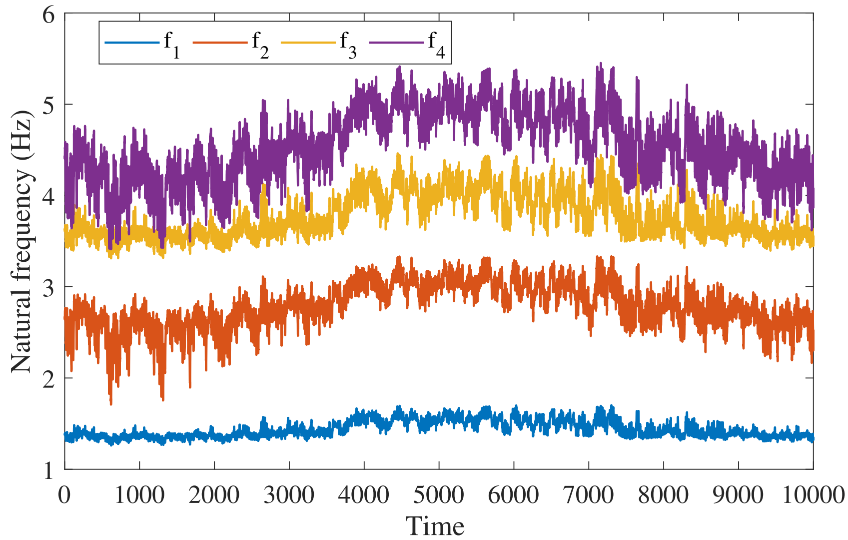


(b)

Figure 5: (a) Hourly recorded temperature of Basel-Switaerland shifted $-15$ $^oC$, and (b) calculated natural frequencies of the spring-mass system for the time period from June 2019 to July 2020.

the augmented Lagrangian in a sequence of iterative sub-optimisations called alternate direction method of multipliers (ADMM) [33]. This makes the VMD a parametric decomposition algorithm urging the users to specify some parameters prior to decomposition as follows,

1. The number of IMFs $k$ to which the original signal is set to be decomposed. In this paper $k$ is set to 2 to remove the seasonal pattern from the frequency time series.
2. The quadratic penalty term $\alpha$ which is a denoising factor. $\alpha$ needs to be set larger when the less noise is tolerated in the decomposition. In this section, $\alpha$ is set to 100 to denoise the frequency signals. [2]
3. Time step $\tau$. In case an exact reconstruction is intended, $\tau$ needs to be set at a small number. In this case, $\tau = 0.1$ is the recommended value by the proposers of VMD [34]. Otherwise, one can set $\tau$ to zero when the reconstruction is not strictly enforced, but encouraged in least-squares sense. Since denoising is intended in this paper, $\tau$ is set to 0.
4. The tolerance parameter $\epsilon$ which controls the convergence of the algorithm and is set to $10^{-7}$ in this paper. Note that different values of $\epsilon$ has been tested and while the results were reasonably accurate by selecting $\epsilon = 10^{-5}$, a value of $10^{-7}$ was eventually selected in the examples of this paper. Note that it will take longer for the VMD algorithm to converge when a smaller value of the $\epsilon$ is selected.
5. *init* which initialises vector $\omega$ (IMFs' center frequencies) and can be either set to 0 (zero initialisation), 1 (uniform initialisation), or 2 (random initialisation). The ways of initialising the center frequencies, however, has a little effect on the decomposition results based on the findings in [35]. Therefore, in this paper $init = 0$.
6. *DC* which determines whether or not the first mode is put and kept at DC, i.e. IMF with zero center frequency. It is recommended that the first mode be kept at DC for the purpose of this paper. Therefore, we set $DC = 1$ (True).

VMD is used to decompose the four natural frequency time series of the spring-mass system into two modes, namely a seasonal and a DC mode. Also, restated, the signals are denoised by setting the quadratic penalty term $\alpha = 100$. Figure 6 shows the decomposed natural frequencies along with their center frequencies. As can be seen from the figure, all first IMFs have zero center frequencies. Interestingly, all the second IMFs have similar center frequencies with an average value of about 0.0439 cycles per hour which is equivalent to almost a full cycle per 24 hours. This is due to the fact that the temperature variation between day and night has a cyclic pattern throughout the year. Therefore, the first IMF corresponding to all decomposition is used

[2] In the experimental sections, $\alpha$ is chosen 10 since a less amount of noise presents in signals.

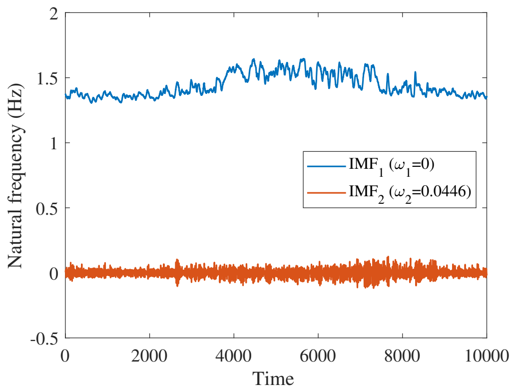


(a) $1^{st}$ frequency

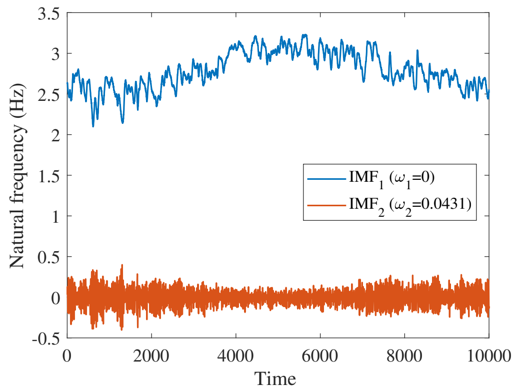


(b) $2^{nd}$ frequency

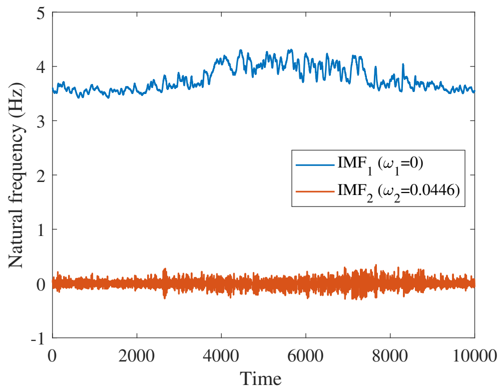


(c) $3^{rd}$ frequency

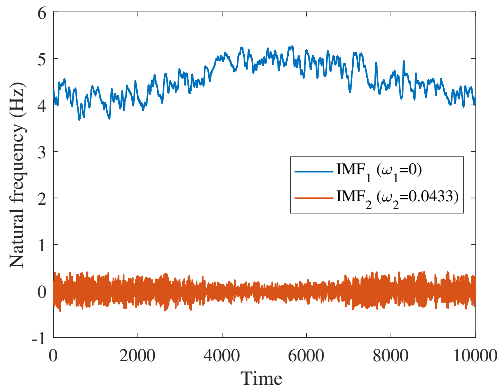


(d) $4^{th}$ frequency

Figure 6: Decomposed natural frequencies of the spring-mass system along with their center frequencies. The first IMF in all cases is kept at DC (zero center frequency).

to construct Johansen CI residuals. However, first, we propose to run the KPSS test on first IMF of each natural frequency time series to explore its stationary/non-stationary nature.

### *4.2. Kwiatkowski–Phillips–Schmidt–Shin (KPSS) test of unit root*

Specifying an appropriate lag length for the KPSS test is essential. A short lag length can make the test biased. In contrast, the power of the test will suffer if the lag length is too large. Therefore, the following equation is used to obtain the maximum lag length [36],

$$L_{\max} = \left[12 \times \left(\frac{N}{100}\right)^{\frac{1}{4}}\right] \tag{14}$$

where $L_{\max}$ is the maximum lag length. $N$ and [.] indicate respectively the sample size (number of observations) and the integer part of a number. Regarding the spring-mass system $n = 10000$ and, therefore, $L_{\max}$ is calculated 37. Table 2 shows the results of the KPSS test run on the first IMF, its corresponding difference form, and the second IMF regarding all the four natural frequency time series of the spring-mass system. Three different lag length, namely 35, 36, and

37, are used. The significance level for the test is set to 0.1. Smaller P-value than the significance level (0.1) indicates that the probability of the type I error is less than the tolerance. This means that the null hypothesis of stationary can be confidently rejected and, therefore, the signal is regarded as non-stationary. The opposite conclusion can be made when the P-value is larger than the significance level. As such, for larger P-value (compared with the significance level) the null hypothesis of stationary cannot be rejected and therefore the signal is regarded as stationary. The results indicate that $\mathrm{IMF}_1$ corresponding to all natural frequency signals is non-stationary in all forms of the signals associated with the specified lag lengths. However, the first difference of the $\mathrm{IMF}_1$ time series is stationary in all cases. This confirms that these signals are of $I(1)$ and, therefore, a Johansen procedure to derive CI residuals can be followed for them. The results also confirm that all $\mathrm{IMF}_2$ time series are stationary in level.

Table 2: The results of the KPSS test run on $\mathrm{IMF}_1$, $\Delta\mathrm{IMF}_1$, and $\mathrm{IMF}_2$ corresponding to all natural frequency time series of the spring-mass system. The significance level for the test is 0.1.

| $1^{st}$ frequency | | | | |
|---|---|---|---|---|
| **Signal** | **Lag** | **P-value** | **h** | **Stationary** |
| $\mathrm{IMF}_1$ | 35, 36, 37 | 0.01, 0.01, 0.01 | 1, 1, 1 | × |
| $\Delta\mathrm{IMF}_1$ | 35, 36, 37 | 0.10, 0.10, 0.10 | 0, 0, 0 | ✓ |
| $\mathrm{IMF}_2$ | 35, 36, 37 | 0.10, 0.10, 0.10 | 0, 0, 0 | ✓ |
| $2^{nd}$ frequency | | | | |
| $\mathrm{IMF}_1$ | 35, 36, 37 | 0.01, 0.01, 0.01 | 1, 1, 1 | × |
| $\Delta\mathrm{IMF}_1$ | 35, 36, 37 | 0.10, 0.10, 0.10 | 0, 0, 0 | ✓ |
| $\mathrm{IMF}_2$ | 35, 36, 37 | 0.10, 0.10, 0.10 | 0, 0, 0 | ✓ |
| $3^{rd}$ frequency | | | | |
| $\mathrm{IMF}_1$ | 35, 36, 37 | 0.01, 0.01, 0.01 | 1, 1, 1 | × |
| $\Delta\mathrm{IMF}_1$ | 35, 36, 37 | 0.10, 0.10, 0.10 | 0, 0, 0 | ✓ |
| $\mathrm{IMF}_2$ | 35, 36, 37 | 0.10, 0.10, 0.10 | 0, 0, 0 | ✓ |
| $4^{th}$ frequency | | | | |
| $\mathrm{IMF}_1$ | 35, 36, 37 | 0.01, 0.01, 0.01 | 1, 1, 1 | × |
| $\Delta\mathrm{IMF}_1$ | 35, 36, 37 | 0.10, 0.10, 0.10 | 0, 0, 0 | ✓ |
| $\mathrm{IMF}_2$ | 35, 36, 37 | 0.10, 0.10, 0.10 | 0, 0, 0 | ✓ |

### *4.3. Johansen cointegration (CI) residuals*

We showed that the first IMF corresponding to all frequency time series is of $I(1)$. Therefore, the Johansen procedure to obtain the CI residuals can be followed. The CI residuals correspond-

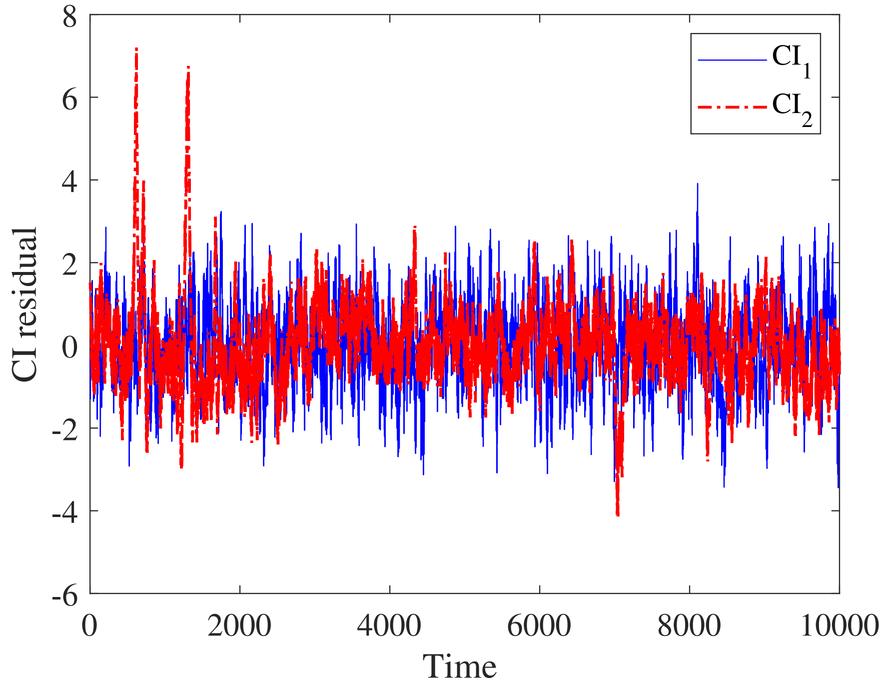


Figure 7: CI residuals obtained from $\mathrm{IMF}_1$ signals corresponding to the frequency time series decomposition of the spring-mass system.

ing to the first two largest eigenvalues of (8) are calculated and used for damage detection in this paper. Figure 7 shows the two obtained CI residuals. Table 3 shows the results of KPSS test run on both CI residuals. The results confirm that the both CI residuals are stationary in level.

Table 3: The results of the KPSS test run CI residuals of the spring-mass system. The significance level for the test is 0.1.

| **Signal** | **Lag** | **P-value** | **h** | **Stationary** |
|---|---|---|---|---|
| $\mathrm{CI}_1$ | 35, 36, 37 | 0.10, 0.10, 0.10 | 0, 0, 0 | ✓ |
| $\mathrm{CI}_2$ | 35, 36, 37 | 0.10, 0.10, 0.10 | 0, 0, 0 | ✓ |

Next, we train a Recurrent Neural Network (RNN) to learn the Johansen CI residuals from the first IMF signals using a 50% of the signals corresponding to the healthy state of the structure. The trained RNN is then used to predict the expected CI residuals in the future. Finally, the results of the predictions are compared against the Johansen CI residuals as discussed in Section 3.

### *4.4. Training a Recurrent Neural Network*

Using Long-Short Term Memory (LSTM) cells have been proven to be effective for forecasting time series [37, 38]. Therefore, in this paper LSTM cells are used in a RNN to learn the underlying

Johansen CI residuals from a portion of the first IMF signals corresponding to the healthy structure. To this end, 50% ($q = 50$ in Figure 3) of the Johansen CI residuals is used as the training targets. Likewise, 50% of the first IMF signals is used as training features. The remaining of the signals is used for testing. It is hypothesised that the error regarding the prediction of the CI residuals will deviate significantly from the average error at the point of the introduction of damage and lasts as long as the damage exists. First, a brief background theory of LSTM cells is explained.

An LSTM unit incorporates three gates: update, forget, and output gates as well as three cells: input, memory, and update cells. The candidate value $\tilde{c}^{<t>}$ to update the memory cell at time $t$ is calculated using the output value at time $t-1$, $a^{<t-1>}$, and the input value at time $t$, $x^{<t>}$ through

$$\tilde{c}^{<t>} = \tanh\left(W_c\left[a^{<t-1>}, x^{<t>}\right] + b_c\right) \tag{15}$$

where tanh(.) represents the hyperbolic tangent activation function. $W_c$ and $b_c$ are respectively the matrix of parameters and biased vector of the memory cell. The candidate value $\tilde{c}^{<t>}$ and the previous value $c^{<t-1>}$ of the cell are then used to update the value of the memory cell $c^{<t>}$ in

$$c^{<t>} = \Gamma_u \odot \tilde{c}^{<t>} + \Gamma_f \odot c^{<t-1>} \tag{16}$$

where

$$\Gamma_u = \sigma\left(W_u\left[a^{<t-1>}, x^{<t>}\right] + b_u\right) \tag{17}$$

and

$$\Gamma_f = \sigma\left(W_f\left[a^{<t-1>}, x^{<t>}\right] + b_f\right) \tag{18}$$

Note that $\odot$ indicates element-wise product of two vectors. $\Gamma_u$ and $\Gamma_f$ are the values of the update and forget gates where $\sigma$ (.) is the sigmoid activation function. $W_u$ and $b_u$ represent respectively the matrix of parameters and the bias vector corresponding to the update gate. Likewise, $W_f$ and $b_f$ are their counterparts corresponding to the forget gate.

Therefore, the output value of the LSTM unit at time $t$ is calculated as

$$a^{<t>} = \Gamma_o \odot \tanh\left(c^{<t>}\right) \tag{19}$$

where

$$\Gamma_o = \sigma\left(W_o\left[a^{<t-1>}, x^{<t>}\right] + b_o\right) \tag{20}$$

in which $\Gamma_o$ is the value of the output gate. $W_o$ and $b_o$ represent respectively the matrix of parameters and bias vector corresponding to the output gate. Figure 8 shows a visualisation of a LSTM unit.

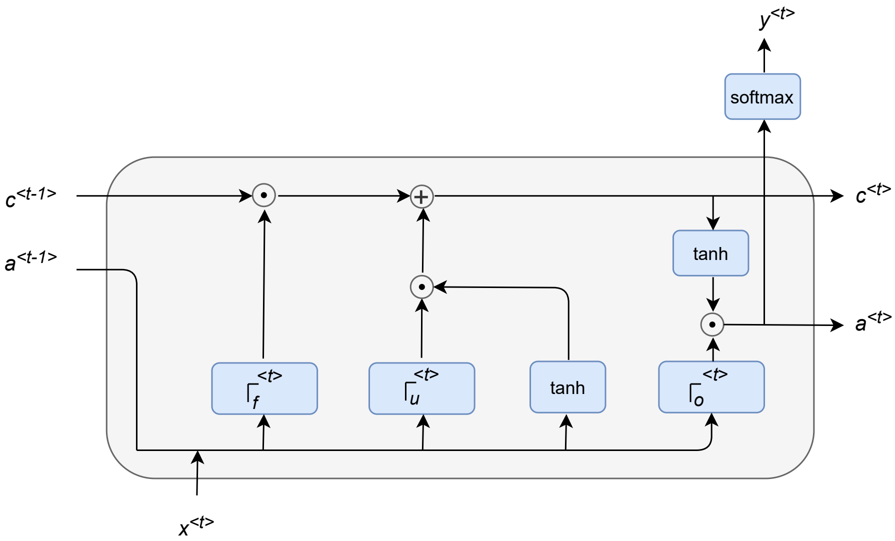


Figure 8: Visualisation of an LSTM unit. $y^{<t>}$ is the final output of the unit at time $t$ which is computed by the softmax activation function.

A multivariate RNN architecture is used which takes the value of four IMFs at time $t$ as input, and outputs the CI residual at the same time. The architecture of the developed stacked RNN follows:

1. a sequence input layer taking four features as inputs.
2. a LSTM layer with 300 units.
3. a fully connected layer with 50 units.
4. a fully connected layer with one output unit.

Adam optimisation is set in options as the optimisation algorithm [39]. The learning rate is set initially at 0.005 and decreased by a factor of 0.2 at every 200 epochs. The number of maximum epochs is chosen 1000. In order to avoid exploding gradients effect, a gradient threshold of 1 is considered in settings.

Figures 9 and 10 show the obtained results of predictions regarding $\mathrm{CI}_1$ and $\mathrm{CI}_2$, respectively. The errors in predictions (Figures 9b and 10b) are calculated as the absolute value of the difference between the RNN predictions and Johansen CI results. As it is evident from Figure 9b, the prediction error deviates significantly from the root mean square error (RMSE) corresponding to the predictions regarding the testing period. The results also confirm that although the damage detection using $\mathrm{CI}_2$ is quite successful, it is not as much successful when $\mathrm{CI}_1$ is used in the procedure of the proposed method. In the next section an experimental example is solved to confirm the ability of the proposed damage detection method in real structures when data from a short-term monitoring of the structure is available.

https://doi.org/10.1016/j.ymssp.2021.107847

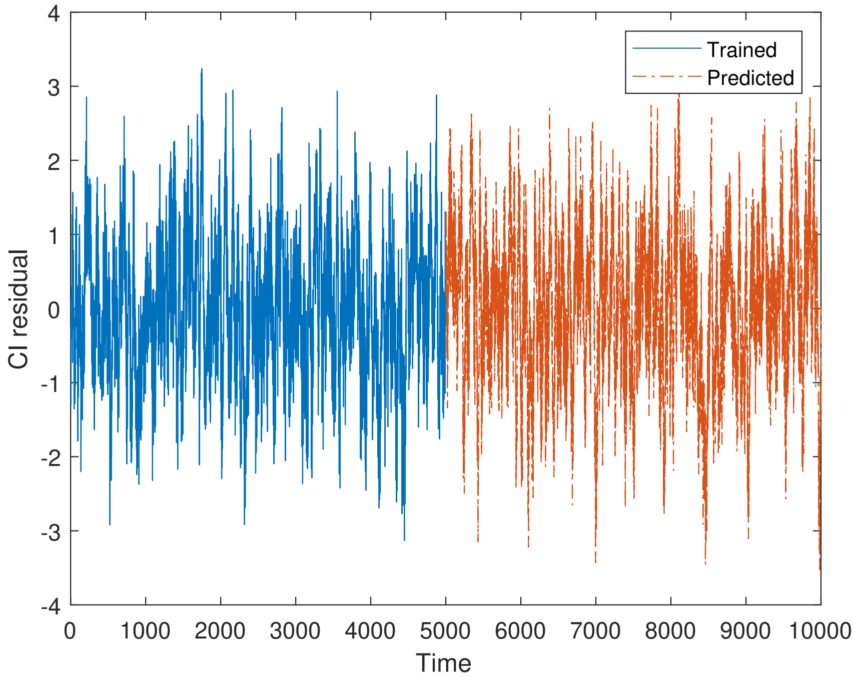


(a) Trained and predicted

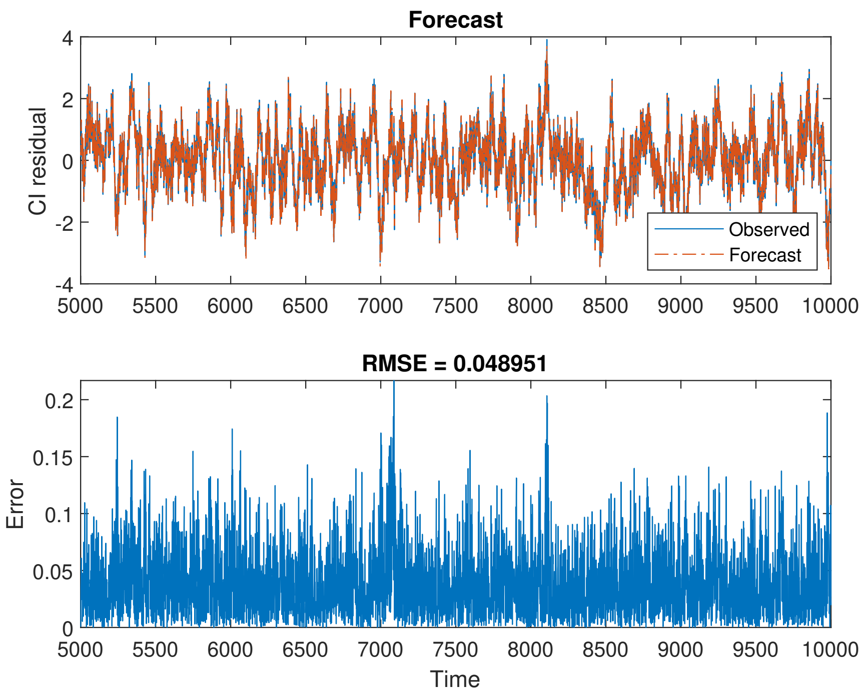


(b) Prediction result and errors

Figure 9: Prediction results obtained from the trained RNN on $\mathrm{CI}_1$ regarding the spring-mass system.

https://doi.org/10.1016/j.ymssp.2021.107847

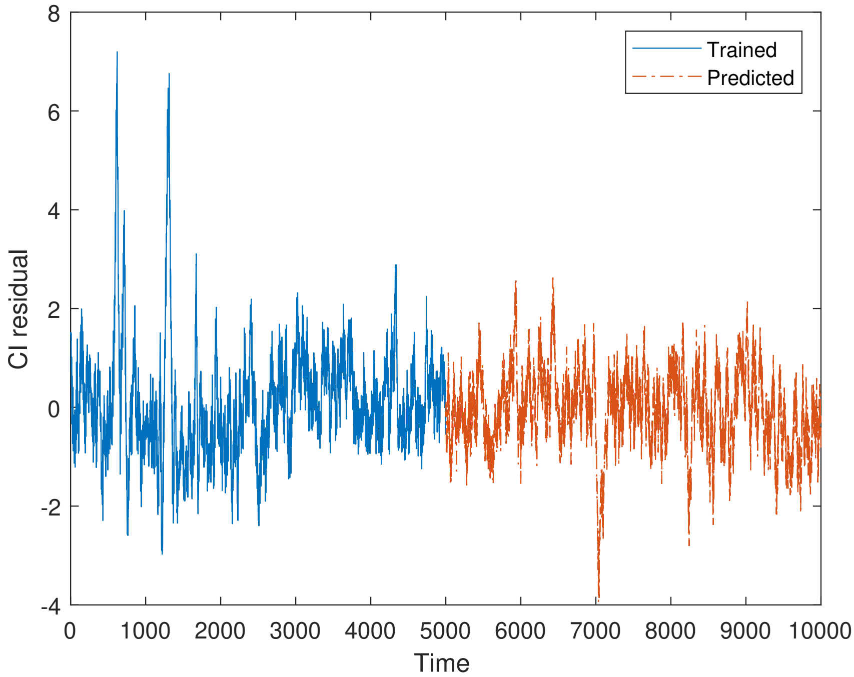


(a) Trained and predicted

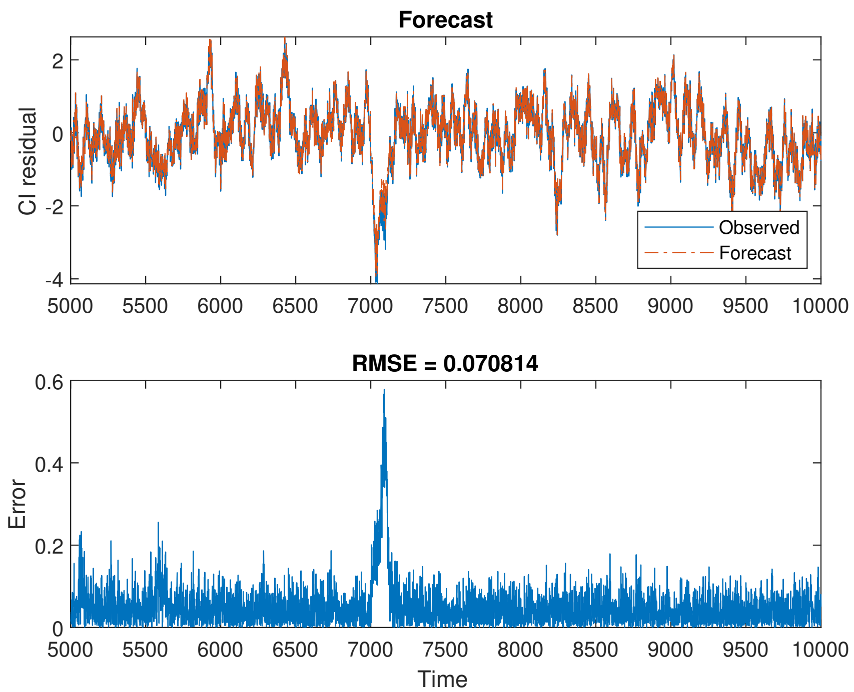


(b) Prediction result and errors

Figure 10: Prediction results obtained from the trained RNN on $CI_2$ regarding the spring-mass system.

## 5. Experimental example (1): Wooden bridge

In this section an experimental example of a wooden bridge model is studied. The source of the data is available online at [40]. Figure 11 shows the picture of the wooden bridge model along with the location of sensors and imposed damage. The readers are referred to the original publications related to this experimental study, however, a brief explanation of the experimental setup and test conditions are presented in the following paragraphs [41, 42, 43].

A random excitation force was applied to the structure in order to excite its lowest modes. Fifteen accelerometers were placed on the structure to measure its response to the excitation force at three different directions. The sampling frequency for the measurements was set at 256 Hz where the measurement period was 32 s. The measured data were first passed through a low-pass filter with the cutoff frequency 64 Hz. The measurements were conducted over several days where the dynamic properties of the structure varied due to environmental changes. These effects were mainly due to the temperature and humidity variations. To simulate damage, point masses of the size 23.5, 47.0, 70.5, 123.2, and 193.7 g were gradually added to the structure. The location of the added masses was the top flange, 600 mm left from the midspan. The last measurements were conducted on the healthy structure (Table 4). The added masses were very small compared to the total weight of the structure (36kg) where even the heaviest added mass was only half a percent of the total mass of the model.

Table 4: The damage scenarios regarding the wooden bridge model. Damage is simulated by adding a point mass to the structure on the top girder.

| Damage scenario | Measurements | Added mass (gr) |
|---|---|---|
| Undamaged | 1-1880 | 0 |
| $D_1$ | 1881-1900 | 23.5 |
| $D_2$ | 1901-1923 | 47 |
| $D_3$ | 1924-1945 | 70.5 |
| $D_4$ | 1946-1965 | 123.16 |
| $D_5$ | 1966-1985 | 193.66 |
| Undamaged | 1986-2008 | 0 |

The stochastic subspace identification technique [44] was used to identify the first nine natural frequency and mode shapes of the bridge from the output-only data [41]. However, only the four lowest natural frequency time series of the model are used for damage detection in this paper (Figure 12).

As the first step, the natural frequency time series are decomposed to two IMFs to remove

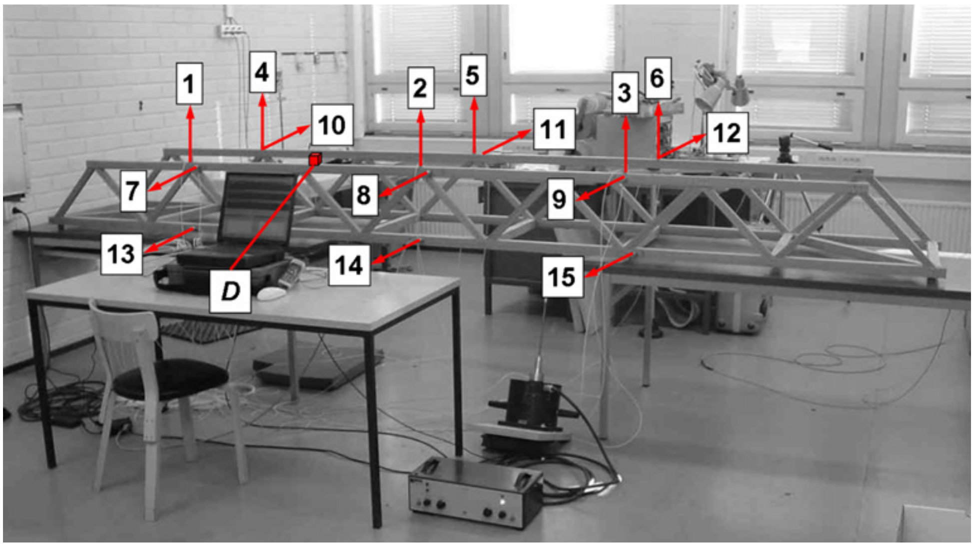


Figure 11: Wooden bridge with the indicated locations of sensors and damage (D) [43].

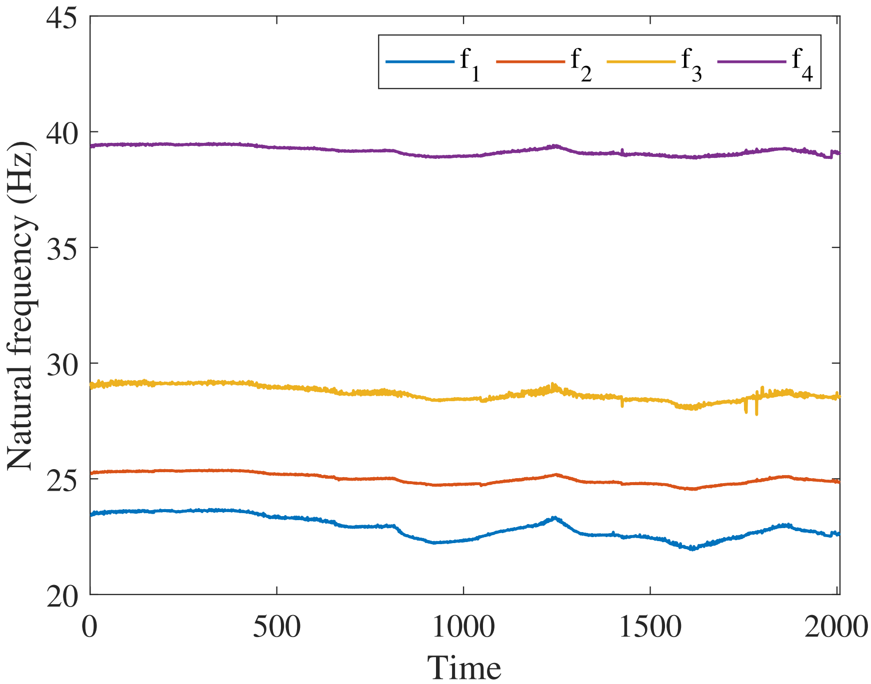


(a)

Figure 12: Calculated four lowest natural frequencies of the wooden bridge model for the time duration of the measurements.

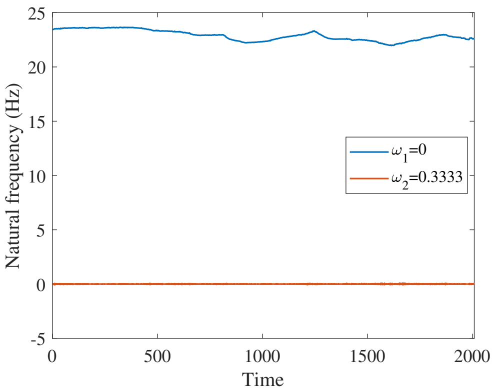


(a) $1^{st}$ frequency

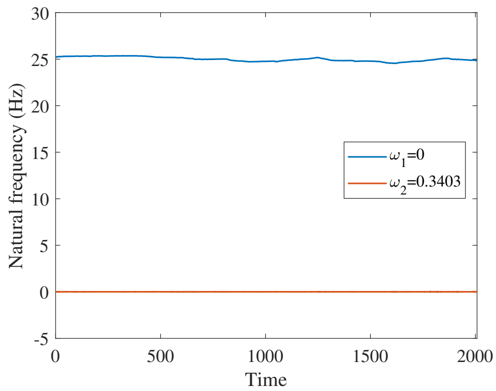


(b) $2^{nd}$ frequency

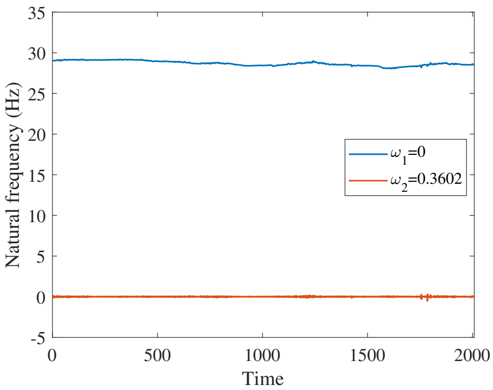


(c) $3^{rd}$ frequency

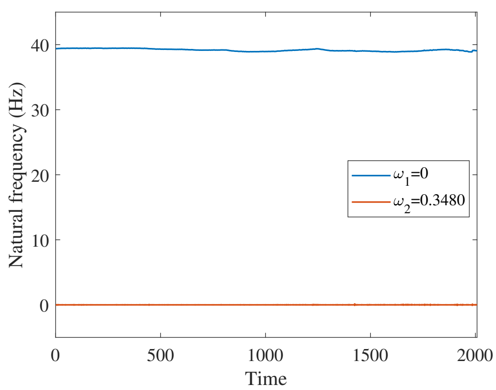


(d) $4^{th}$ frequency

Figure 13: Decomposed natural frequencies of the wooden bridge model along with their center frequencies. The first IMF in all cases is kept at DC (zero center frequency).

the seasonal patterns in the signals. Note that since the data used in this section are less noisy, compared to the numerical example of Section 4, a relatively small value of 10 was chosen for the quadratic penalty term $\alpha$ in VMD settings. Note that the other settings are unchanged. Figure 13 shows the results of the decomposition along with IMFs' center frequencies. Restated, the first IMFs are kept at DC (zero center frequency).

Next, the KPSS test is run on both IMFs regarding the VMD decomposition of each natural frequency time series. A maximum lag 25 was calculated based on the length of the time series, i.e. 2008, using (14). Therefore, three different lag length of 23, 24, and 25 were used for the test. As can be seen from the results presented in Table 5, all the first IMFs are $I(1)$ signals and, therefore, Johansen CI procedure can be applied to them. Also the results confirm that all the second IMFs are of $I(0)$.

Figure 14 shows the two CI residual time series regarding application of the Johansen procedure to the first IMF time series. Next, we run the KPSS test on these residuals. Table 6 shows

Table 5: The results of the KPSS test run on $\mathrm{IMF}_1$, $\Delta\mathrm{IMF}_1$, and $\mathrm{IMF}_2$ corresponding to all natural frequency time series of the wooden bridge model. The significance level for the test is 0.1.

| $1^{st}$ frequency | | | | |
|---|---|---|---|---|
| **Signal** | **Lag** | **P-value** | **h** | **Stationary** |
| $\mathrm{IMF}_1$ | 23, 24, 25 | 0.01, 0.01, 0.01 | 1, 1, 1 | ✗ |
| $\Delta\mathrm{IMF}_1$ | 23, 24, 25 | 0.10, 0.10, 0.10 | 0, 0, 0 | ✓ |
| $\mathrm{IMF}_2$ | 23, 24, 25 | 0.10, 0.10, 0.10 | 0, 0, 0 | ✓ |
| $2^{nd}$ frequency | | | | |
| $\mathrm{IMF}_1$ | 23, 24, 25 | 0.01, 0.01, 0.01 | 1, 1, 1 | ✗ |
| $\Delta\mathrm{IMF}_1$ | 23, 24, 25 | 0.10, 0.10, 0.10 | 0, 0, 0 | ✓ |
| $\mathrm{IMF}_2$ | 23, 24, 25 | 0.10, 0.10, 0.10 | 0, 0, 0 | ✓ |
| $3^{rd}$ frequency | | | | |
| $\mathrm{IMF}_1$ | 23, 24, 25 | 0.01, 0.01, 0.01 | 1, 1, 1 | ✗ |
| $\Delta\mathrm{IMF}_1$ | 23, 24, 25 | 0.10, 0.10, 0.10 | 0, 0, 0 | ✓ |
| $\mathrm{IMF}_2$ | 23, 24, 25 | 0.10, 0.10, 0.10 | 0, 0, 0 | ✓ |
| $4^{th}$ frequency | | | | |
| $\mathrm{IMF}_1$ | 23, 24, 25 | 0.01, 0.01, 0.01 | 1, 1, 1 | ✗ |
| $\Delta\mathrm{IMF}_1$ | 23, 24, 25 | 0.10, 0.10, 0.10 | 0, 0, 0 | ✓ |
| $\mathrm{IMF}_2$ | 23, 24, 25 | 0.10, 0.10, 0.10 | 0, 0, 0 | ✓ |

the results. Accordingly, both obtained CI time series are of $I(1)$. This means that there is no linear combination of the first IMF time series which is stationary. However, this will not stop us from pursuing further with our proposed strategy.

Table 6: The results of the KPSS test run CI residuals of the wooden bridge model. The significance level for the test is 0.1.

| **Signal** | **Lag** | **P-value** | **h** | **Stationary** |
|---|---|---|---|---|
| $\mathrm{CI}_1$ | 23, 24, 25 | 0.01, 0.01, 0.01 | 1, 1, 1 | ✗ |
| $\mathrm{CI}_2$ | 23, 24, 25 | 0.01, 0.01, 0.01 | 1, 1, 1 | ✗ |

Next, we train a RNN to learn the CI relationship obtained through using Johansen procedure. Note the architecture used to this end is identical to the one in Section 4.4 except for the first layer where 400 LSTM units are used in here. All the other settings are kept unchanged as well. Likewise to the problem of Section 4, 50% of the data are used as training set and the rest are used for testing as illustrated in Figures 15a and 16a. Figures 15 and 16 show the

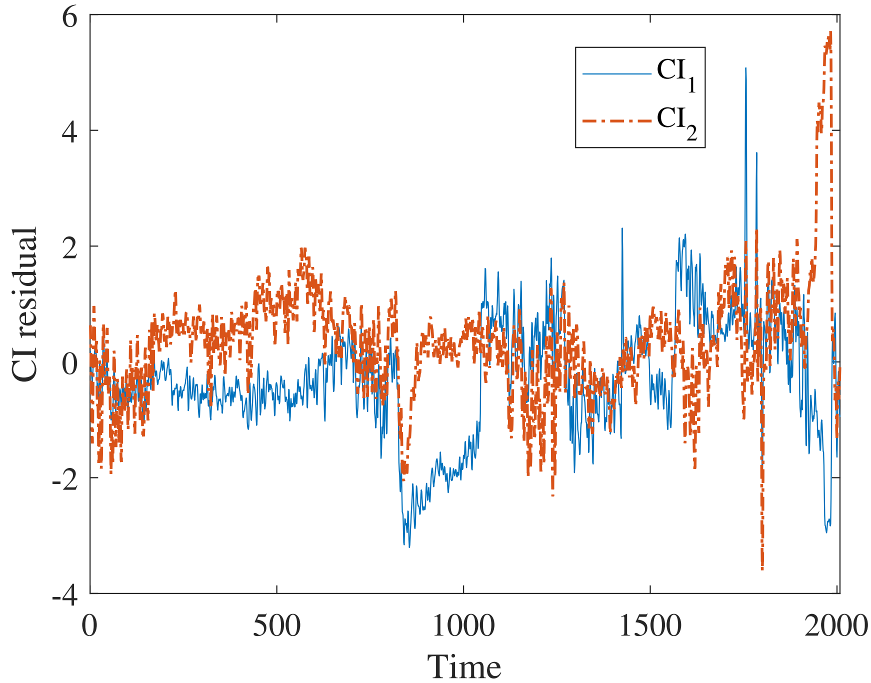


Figure 14: CI residuals obtained from $IMF_1$ signals corresponding to the frequency time series decomposition of wooden bridge model.

obtained results. As is evident from the results, similar to the results obtained in Section 4, damage detection is not possible using $CI_1$. However, the procedure of the damage detection is fairly satisfactory using $CI_2$. As can be seen the prediction error deviates from the average error significantly in this case. Also the prediction error goes back to normal when the damage does not exist for the measurement period 1986-2008. The results of the damage detection are comparable to the one in [41]. Another interesting observation is that the prediction error regarding $CI_1$ seems to provide a decent threshold setting for the prediction problem of $CI_2$. As can be seen from Figure 15, the maximum error of the prediction of $CI_1$ is 0.2174. The same conclusion can be made as for the numerical example of Section 4.

## 6. Experimental example (2): bridge Z24

The Z24 Bridge is a well-known benchmark problem that has been used to investigate the possibility of long-term structural health monitoring under EOV effects [45, 46, 47]. The problem is of particular interest due to the existence of non-linear relationships among natural frequencies during a period of very cold temperatures [30].

Figure 17 shows the geographical location of the bridge Z24. The bridge was a classical post-tensioned concrete two-cell box-girder with a main span of 30 m and two side spans of 14 m. The monitoring campaign was established one year prior to the bridge dismantlement. During this

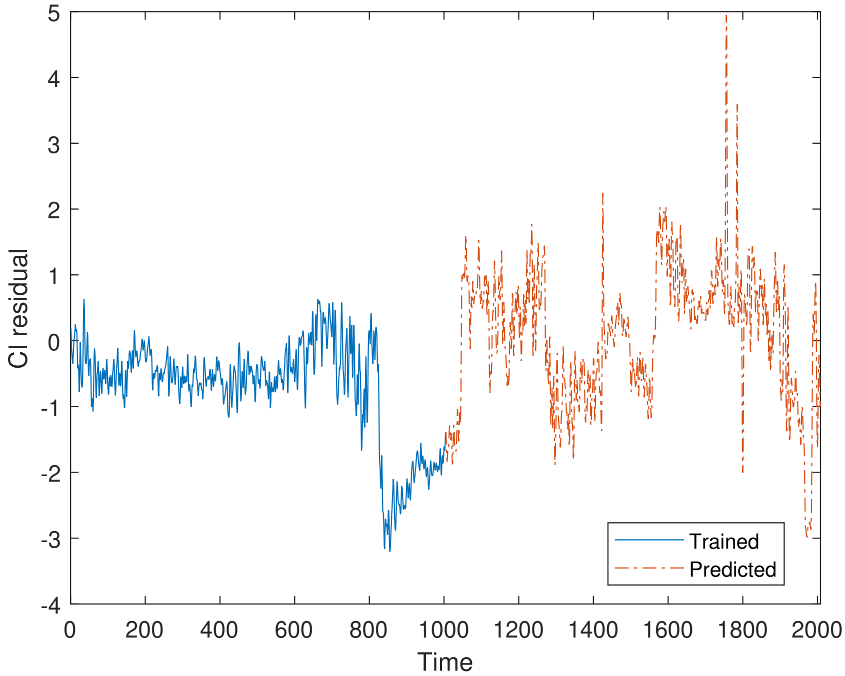


(a) Trained and predicted

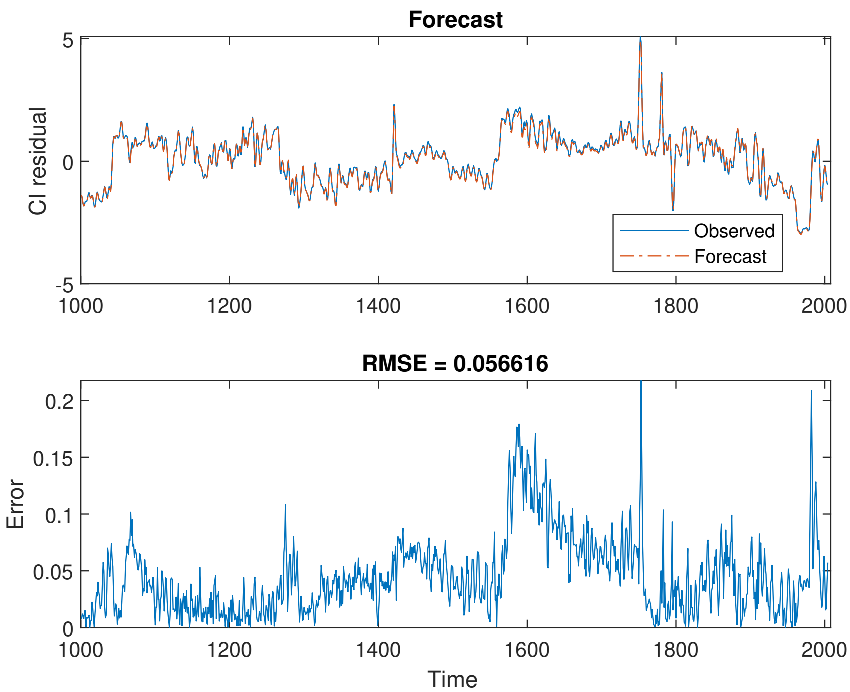


(b) Prediction result and errors

Figure 15: Prediction results obtained from the trained RNN on $CI_1$ regarding the wooden bridge model.

https://doi.org/10.1016/j.ymssp.2021.107847

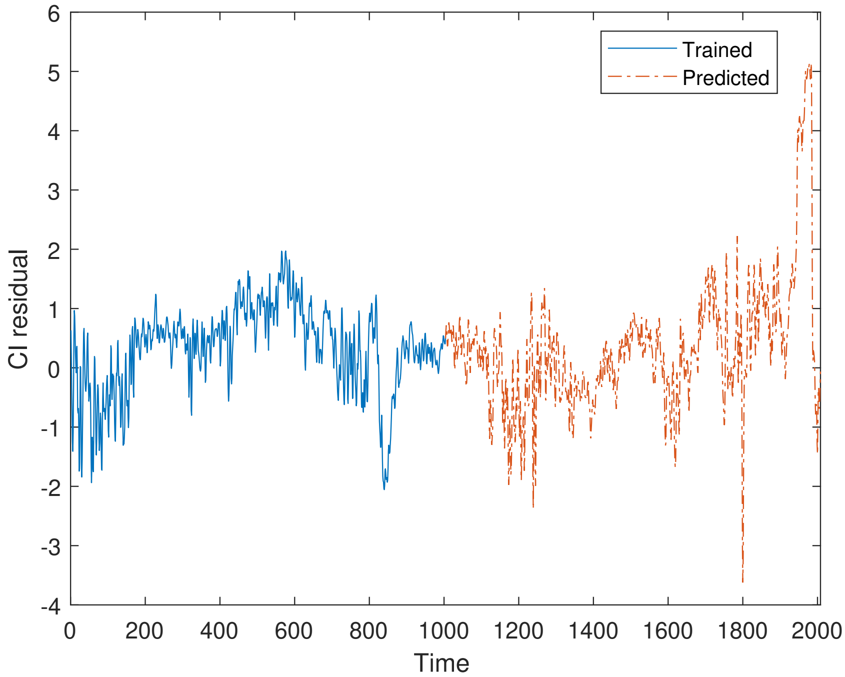


(a) Trained and predicted

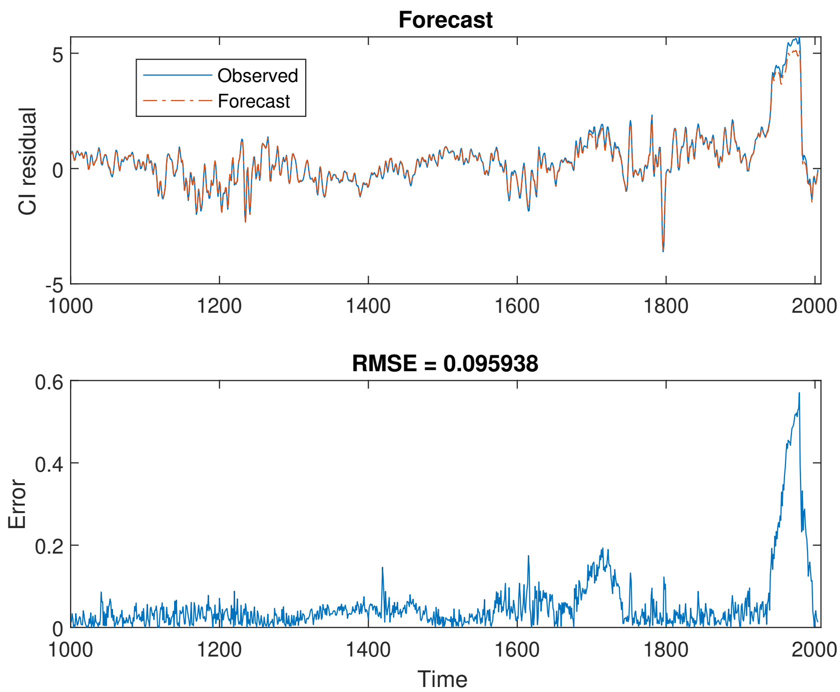


(b) Prediction result and errors

Figure 16: Prediction results obtained from the trained RNN on $CI_2$ regarding the wooden bridge model.

https://doi.org/10.1016/j.ymssp.2021.107847

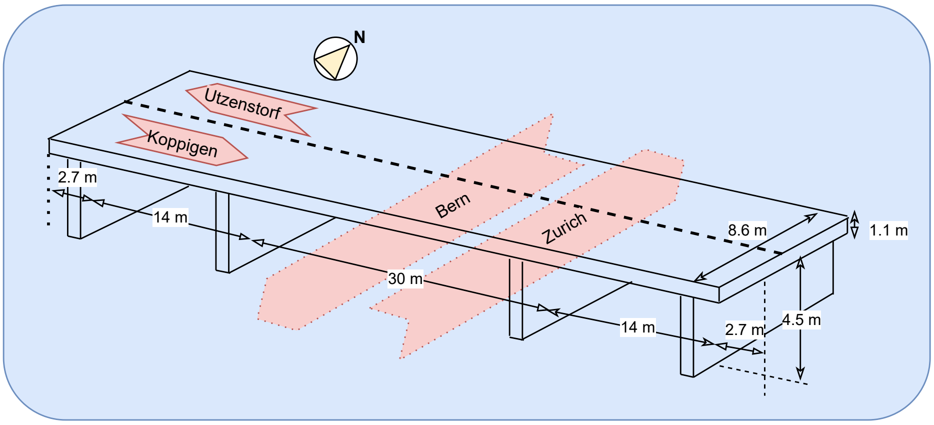


Figure 17: Bridge Z24 geometry and location.

period, several damage scenarios were implemented to simulate a progressing damage scenario where damage introduced progressively over a long period of time. Since the effect of EOV on structural dynamics was known, the meteorological parameters were also monitored during this period in full details.

The number of 16 accelerameters were installed at different locations and directions on the bridge to record 8 averages of 8192 acceleration samples per hour. The bridge first four natural frequencies were calculated using the recorded vibration data. Moreover, 48 sensors were used to record 10 scans of environmental data in every hour. However, since there are some missing data in the original dataset, the points pertinent to the corresponding time instants are all removed, as suggested in [30], as a data pre-processing stage. As a result, the number of 3932 data-points remains. Figures 18a and 18b show respectively the air temperature profile as well as the corresponding first four natural frequency time series of the bridge obtained from the measured vibration signal during this period. For more details, the readers are referred to [48, 49].

First, VMD is used to remove the seasonal effects in the frequency signals. To this end, the same parameters, as those in Section 5, are used in the VMD setting in here. Figure 19 depicts the obtained IMFs along with their corresponding center frequencies. Likewise to the previous sections, the first IMFs are kept at DC (zero center frequency). Next, the KPSS test is run on $\mathrm{IMF}_1$, $\Delta\mathrm{IMF}_1$, and $\mathrm{IMF}_2$, the results of which are presented in Table 7. A maximum lag of 30 is obtained using (14) and three different lags, i.e. 28, 29, 30, are used to this end. As can be seen from the table, all $\mathrm{IMF}_1$ signals are non-stationary whereas their corresponding $\Delta$ variant is stationary. This confirms that all $\mathrm{IMF}_1$ signals are of $I(1)$. All the $\mathrm{IMF}_2$ signals, however, are stationary in level.

Figure 20 shows the two CI residuals obtained from the $\mathrm{IMF}_1$ signals. Table 8 shows the results of the KPSS test run on both CI signals. As can be seen from the table, $\mathrm{CI}_1$ is stationary

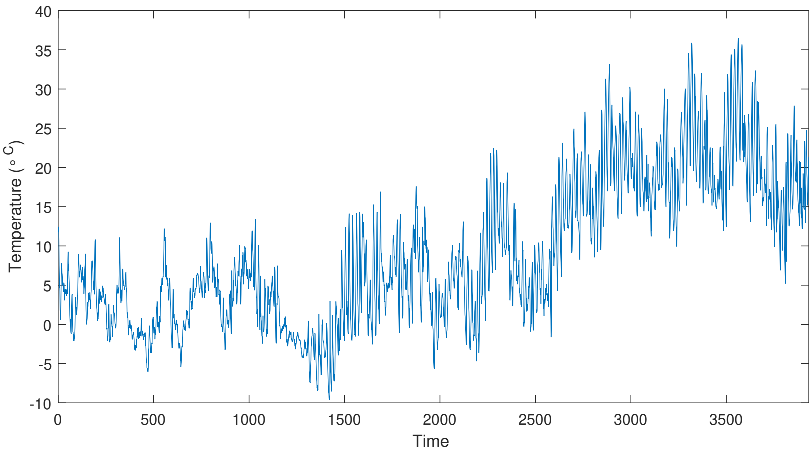


(a)

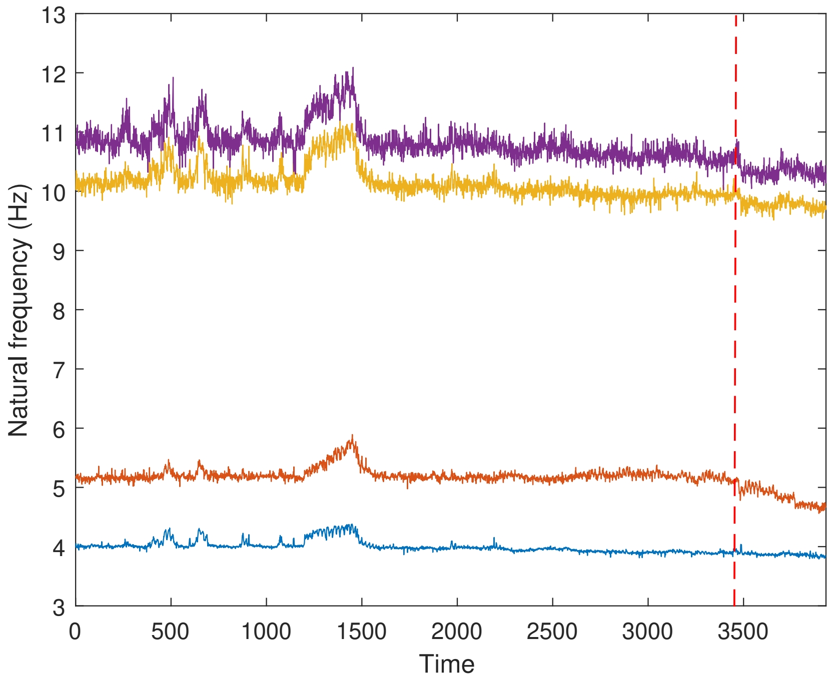


(b)

Figure 18: (a) Hourly recorded air temperature of regarding Z24 bridge (b) obtained natural frequencies of the Z24 bridge where the dashed line indicates the time when damage started to be introduced.

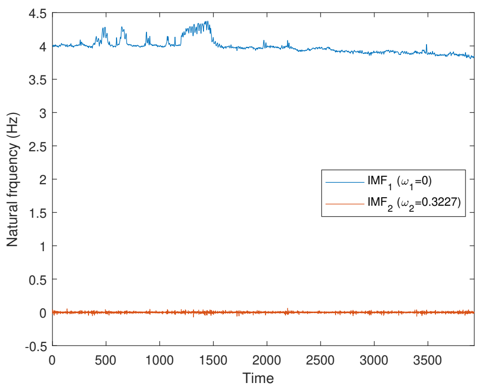


(a) $1^{st}$ frequency

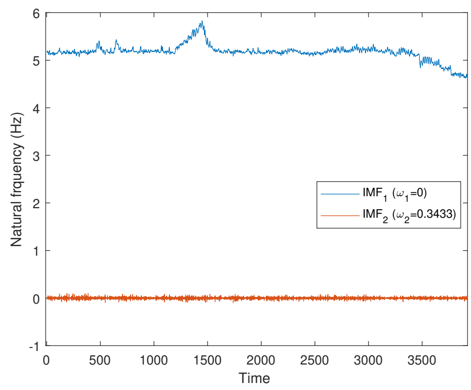


(b) $2^{nd}$ frequency

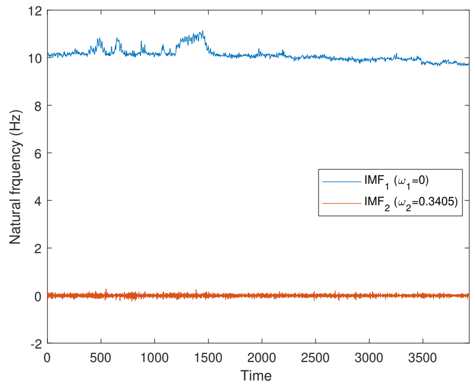


(c) $3^{rd}$ frequency

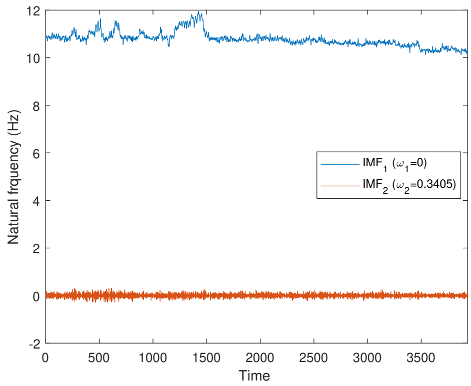


(d) $4^{th}$ frequency

Figure 19: Decomposed natural frequencies of the bridge Z24 along with their center frequencies. The first IMF in all cases is kept at DC (zero center frequency).

while $\mathrm{CI}_2$ is non-stationary. This is compatible with the fact that the CI corresponding to the largest eigenvalue of (8), i.e. $\mathrm{CI}_1$, is the most stationary signal [30]. Next, the obtained CI signals along with the $\mathrm{IMF}_1$ signals are respectively used as targets and features to train two separate RNNs using 50% of the dataset corresponding to the healthy state of the structure ($q = 50$ in Figure 3). The results of which are presented respectively as for $\mathrm{CI}_1$ and $\mathrm{CI}_2$ in Figures 21 and 22. The dashed line in both cases indicates the time instant when the damage started to be introduced to the structure.

The RNN architecture used in this section is similar to the previous sections except 250 LSTM cells were used in the first layer. The settings are also remained unchanged. The prediction results of both RNNs demonstrate that the damage can be successfully tracked down via monitoring the errors. More interestingly, the error progressively increases which can be further interpreted as damage being introduced to the structure progressively. However, despite the two previous examples of the spring-mass system and wooden bridge, the error corresponding to the prediction

Table 7: The results of the KPSS test run on $\text{IMF}_1$, $\Delta\text{IMF}_1$, and $\text{IMF}_2$ corresponding to all natural frequency time series of the bridge Z24. The significance level for the test is 0.1.

| $1^{st}$ frequency | | | | |
|---|---|---|---|---|
| **Signal** | **Lag** | **P-value** | **h** | **Stationary** |
| $\text{IMF}_1$ | 28, 29, 30 | 0.01, 0.01, 0.01 | 1, 1, 1 | × |
| $\Delta\text{IMF}_1$ | 28, 29, 30 | 0.10, 0.10, 0.10 | 0, 0, 0 | ✓ |
| $\text{IMF}_2$ | 28, 29, 30 | 0.10, 0.10, 0.10 | 0, 0, 0 | ✓ |
| $2^{nd}$ frequency | | | | |
| $\text{IMF}_1$ | 28, 29, 30 | 0.01, 0.01, 0.01 | 1, 1, 1 | × |
| $\Delta\text{IMF}_1$ | 28, 29, 30 | 0.10, 0.10, 0.10 | 0, 0, 0 | ✓ |
| $\text{IMF}_2$ | 28, 29, 30 | 0.10, 0.10, 0.10 | 0, 0, 0 | ✓ |
| $3^{rd}$ frequency | | | | |
| $\text{IMF}_1$ | 28, 29, 30 | 0.01, 0.01, 0.01 | 1, 1, 1 | × |
| $\Delta\text{IMF}_1$ | 28, 29, 30 | 0.10, 0.10, 0.10 | 0, 0, 0 | ✓ |
| $\text{IMF}_2$ | 28, 29, 30 | 0.10, 0.10, 0.10 | 0, 0, 0 | ✓ |
| $4^{th}$ frequency | | | | |
| $\text{IMF}_1$ | 28, 29, 30 | 0.01, 0.01, 0.01 | 1, 1, 1 | × |
| $\Delta\text{IMF}_1$ | 28, 29, 30 | 0.10, 0.10, 0.10 | 0, 0, 0 | ✓ |
| $\text{IMF}_2$ | 28, 29, 30 | 0.10, 0.10, 0.10 | 0, 0, 0 | ✓ |

of $\text{CI}_1$ is more significant when damages occurs. This highlights the point that one needs to consider both CI signals for damage detection using the proposed strategy.

The results obtained from the condition monitoring of the bridge Z24 using the proposed method is fairly comparable to the results obtained in some of the recently proposed techniques such as [30]. The proposed method uses only the four lowest natural frequency signals of the structure as opposed to using a combination of the natural frequency and the mode shape signals used, for example, in some classical techniques (e.g. see [7]).

## 7. Conclusions

A novel structural health monitoring strategy has been proposed to detect changes in the structural response due to damage under environmental and operational variations. The proposed monitoring algorithm can successfully mask the effect of the EOV and raise an early alarm when the structure undergoes damage. Since, identifying the higher structural modes is fairly challenging, if not impossible, only four natural frequency time series of the structure under

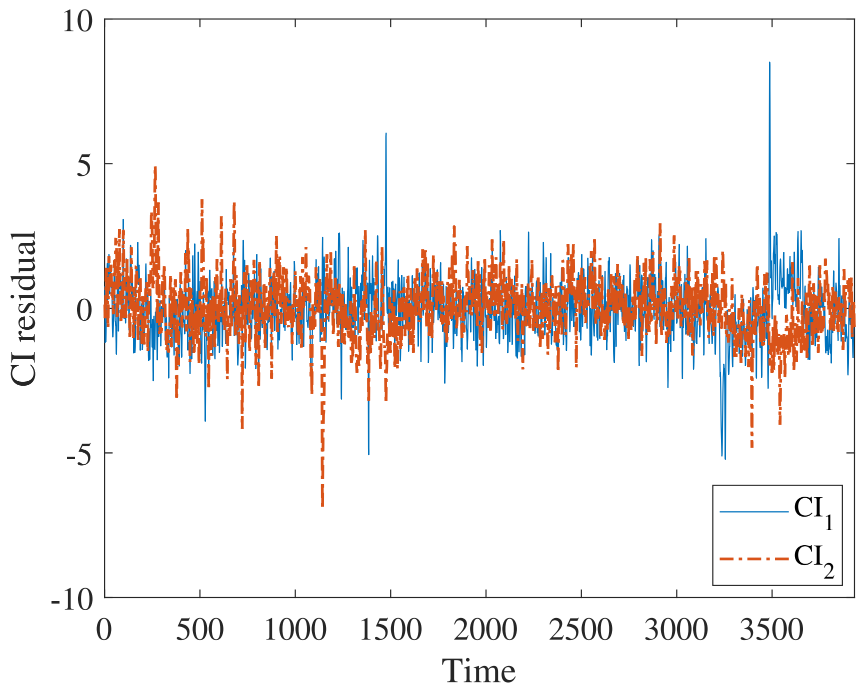


Figure 20: CI residuals obtained from the $IMF_1$ signals corresponding to the frequency time series decomposition of the bridge Z24.

Table 8: The results of the KPSS test run on CI residuals of the bridge Z24. The significance level for the test is 0.1.

| Signal | Lag | P-value | h | Stationary |
|---|---|---|---|---|
| $CI_1$ | 28, 29, 30 | 0.0896, 0.0933, 0.0968 | 0, 0, 0 | ✓ |
| $CI_2$ | 28, 29, 30 | 0.01, 0.01, 0.01 | 1, 1, 1 | × |

studies were used in this paper for damage detection. However, the possibility of using even less number of modes can be a subject of future work. Some of the main outcomes of this paper follows,

1. VMD has been used successfully for denoising and removing of the seasonal patterns in the frequency time series, providing the first IMFs of these time series suitable for conducting Johansen CI test. For instance, the results obtained from the highly noisy simulated frequency signals in Section 4 (10% noise) demonstrate the capability of the proposed method in condition monitoring of structures using highly noisy data. This can be regarded as a strong feature of the proposed strategy compared to other methods where 2% noise was only introduced into simulations (e.g. see [30]).
2. The proposed method has been proven to be successful through both a numerical and two experimental studies. It was shown that, regarding the wooden bridge example, the

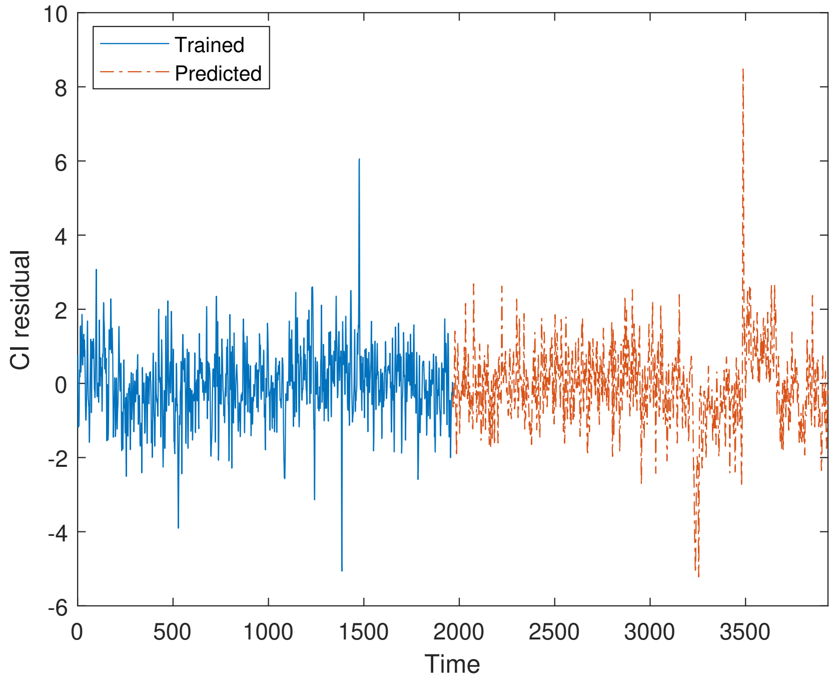


(a) Trained and predicted

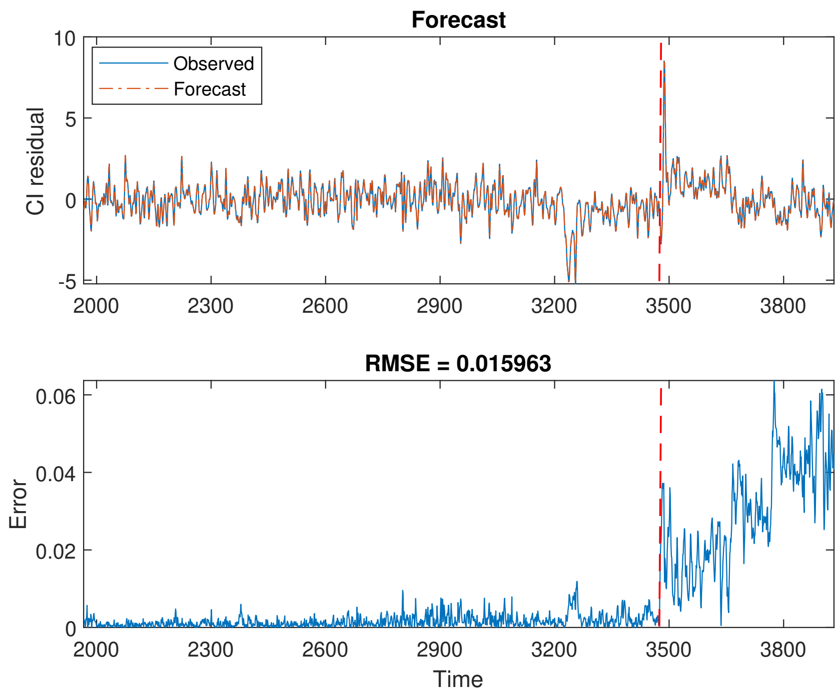


(b) Prediction result and errors

Figure 21: Prediction results obtained from the trained RNN on $CI_1$ regarding the bridge z24.

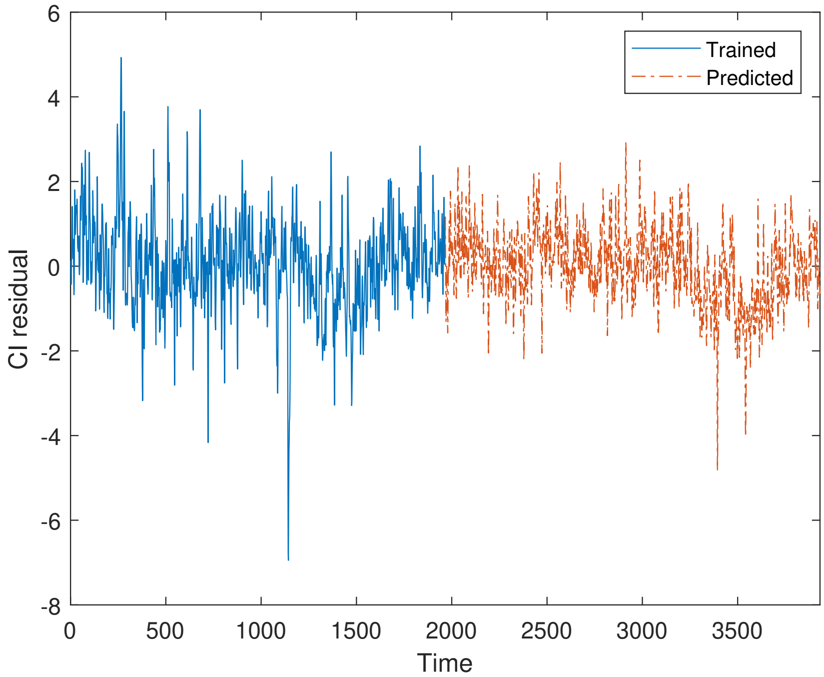


(a) Trained and predicted

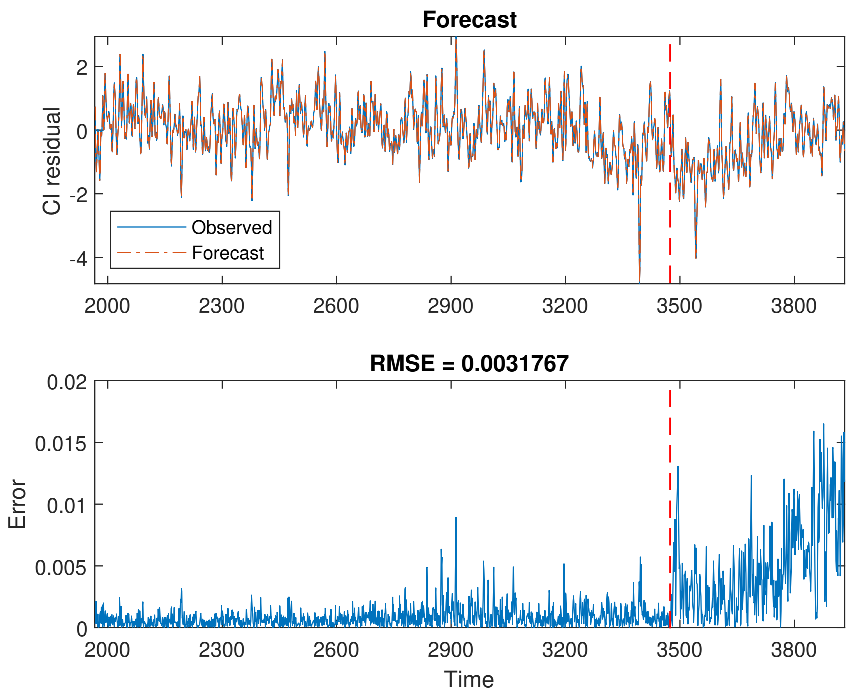


(b) Prediction result and errors

Figure 22: Prediction results obtained from the trained RNN on $CI_2$ regarding the bridge z24.

proposed monitoring strategy can still be successfully applied even when the Johansen CI fails to obtain a stationary combination of the signals.

3. It was shown that the prediction of the $CI_2$ using a trained RNN deviates from the average error significantly, regarding the examples of Section 4 and 5, when the damage occurs in the system. This error was shown to come back to normal when the damage is removed. This is an important outcome since it shows that the trained RNN can be still used for monitoring the structure after when the damage is fixed. In Section 6, the condition monitoring of the structure was possible using monitoring of the prediction errors of both CIs. However, better results were achieved using $CI_1$.
4. Regarding the two previous observations, it seems that the proposed strategy favours using a less stationary combination of the signals in some cases (Sections 4 and 5) and, therefore, one may not need to use any non-linear CI rather than Johansen procedure to use the proposed method. Future work can be dedicated, however, to further investigation of this statement.
5. It was noted that the error of the prediction of $CI_1$ residuals can provide a threshold for the prediction of $CI_2$ when $CI_2$ is more suitable for damage detection. This is fairly evident from both the numerical and experimental studies of Sections 4 and 5.

The proposed monitoring strategy was tested on an experimental example where data from a short-run (a couple of days) monitoring of the structure was available (Section 5). Regarding the results, the proposed damage detection strategy is superior to many other methods that need a long-term monitoring data to train non-linear CI residuals to be used for damage detection [26].

## Acknowledgement

The KU Leuven Structural Mechanics Section is acknowledged as the source of the data for bridge Z24.

## References

[1] O. C. Zienkiewicz, R. L. Taylor, J. Z. Zhu, The finite element method: its basis and fundamentals, Elsevier, 2013.

[2] C. Liu, J. T. DeWolf, Effect of temperature on modal variability of a curved concrete bridge under ambient loads, Journal of structural engineering 133 (12) (2007) 1742–1751.

[3] G. Feltrin, Temperature and damage effects on modal parameters of a reinforced concrete bridge, in: Proc., 4th Int. Conf. on Structural Dynamics, Eurodyn 2002, Balkema, 2002, pp. 373–378.

[4] C. Rainieri, F. Magalhaes, D. Gargaro, G. Fabbrocino, A. Cunha, Predicting the variability of natural frequencies and its causes by second-order blind identification, Structural Health Monitoring 18 (2) (2019) 486–507.

[5] A. A. Mosavi, R. Seracino, S. Rizkalla, Effect of temperature on daily modal variability of a steel-concrete composite bridge, Journal of Bridge Engineering 17 (6) (2012) 979–983.

[6] C. R. Farrar, H. Sohn, K. Worden, Data normalization: a key for structural health monitoring, Tech. rep., Los Alamos National Lab., NM (US) (2001).

[7] J. Kullaa, Damage detection of the z24 bridge using control charts, Mechanical Systems and Signal Processing 17 (1) (2003) 163–170.

[8] E. J. Cross, K. Worden, Q. Chen, Cointegration: a novel approach for the removal of environmental trends in structural health monitoring data, Proceedings of the Royal Society A: Mathematical, Physical and Engineering Sciences 467 (2133) (2011) 2712–2732.

[9] A. Banerjee, J. J. Dolado, J. W. Galbraith, D. Hendry, et al., Co-integration, error correction, and the econometric analysis of non-stationary data, OUP Catalogue (1993).

[10] E. J. Cross, K. Worden, Cointegration and why it works for shm, in: Journal of Physics: Conference Series, Vol. 382, IOP Publishing, 2012, p. 012046.

[11] P. B. Dao, W. J. Staszewski, Data normalisation for lamb wave–based damage detection using cointegration: A case study with single-and multiple-temperature trends, Journal of intelligent material systems and structures 25 (7) (2014) 845–857.

[12] B. Golchinfar, M. G. Ramezani, D. Donskoy, H. Saboonchi, Vibro-acoustic modulation technique comparison with conventional nondestructive evaluation methods, in: Health Monitoring of Structural and Biological Systems IX, Vol. 11381, International Society for Optics and Photonics, 2020, p. 113811W.

[13] P. B. Dao, A. Klepka, Ł. Pieczonka, F. Aymerich, W. J. Staszewski, Impact damage detection in smart composites using nonlinear acoustics—cointegration analysis for removal of undesired load effect, Smart Materials and Structures 26 (3) (2017) 035012.

[14] G. P. Dwyer, The johansen tests for cointegration, White Paper (2015).

[15] X. Li, W. Qu, L. Xiao, Y. Lu, Removal of temperature effect in impedance-based damage detection using the cointegration method, Journal of Intelligent Material Systems and Structures 30 (15) (2019) 2189–2197.

[16] E. S. Tomé, M. Pimentel, J. Figueiras, Damage detection under environmental and operational effects using cointegration analysis–application to experimental data from a cable-stayed bridge, Mechanical Systems and Signal Processing 135 (2020) 106386.

[17] A. Michalak, J. Wodecki, A. Wyłomańska, R. Zimroz, Application of cointegration to vibration signal for local damage detection in gearboxes, Applied Acoustics 144 (2019) 4–10.

[18] K. Zolna, P. B. Dao, W. J. Staszewski, T. Barszcz, Towards homoscedastic nonlinear cointegration for structural health monitoring, Mechanical Systems and Signal Processing 75 (2016) 94–108.

[19] E. Cross, K. Worden, Nonlinear cointegration as a combinatorial optimisation problem, Structural Health Monitoring 2011 (2011).

[20] E. J. Cross, K. Worden, Approaches to nonlinear cointegration with a view towards applications in shm, in: Journal of Physics-Conference Series, Vol. 305, 2011, p. 012069.

[21] K. Zolna, P. B. Dao, W. J. Staszewski, T. Barszcz, Nonlinear cointegration approach for condition monitoring of wind turbines, Mathematical Problems in Engineering 2015 (2015).

[22] H. Shi, K. Worden, E. Cross, A nonlinear cointegration approach with applications to structural health monitoring, in: Journal of Physics: Conference Series, Vol. 744, Institute of Physics, 2016.

[23] T. Van Gestel, M. Espinoza, B. Baesens, J. A. Suykens, C. Brasseur, B. De Moor, A bayesian nonlinear support vector machine error correction model, Journal of forecasting 25 (2) (2006) 77–100.

[24] G. Coletta, G. Miraglia, M. Pecorelli, R. Ceravolo, E. Cross, C. Surace, K. Worden, Use of the cointegration strategies to remove environmental effects from data acquired on historical buildings, Engineering Structures 183 (2019) 1014–1026.

[25] H. Shi, K. Worden, E. J. Cross, A cointegration approach for heteroscedastic data based on a time series decomposition: an application to structural health monitoring, Mechanical Systems and Signal Processing 120 (2019) 16–31.

[26] J.-z. Huang, D.-s. Li, H.-n. Li, G.-b. Song, Y. Liang, Damage identification of a large cable-stayed bridge with novel cointegrated kalman filter method under changing environments, Structural Control and Health Monitoring 25 (5) (2018) e2152.

[27] K. Dragomiretskiy, D. Zosso, Variational mode decomposition, IEEE transactions on signal processing 62 (3) (2013) 531–544.

[28] K. Worden, C. R. Farrar, G. Manson, G. Park, The fundamental axioms of structural health monitoring, Proceedings of the Royal Society A: Mathematical, Physical and Engineering Sciences 463 (2082) (2007) 1639–166.

[29] J. L. Doob, Stochastic processes, Vol. 101, New York Wiley, 1953.

[30] H. Shi, K. Worden, E. J. Cross, A regime-switching cointegration approach for removing environmental and operational variations in structural health monitoring, Mechanical Systems and Signal Processing 103 (2018) 381–397.

[31] Weather history download basel (Retrieved August 18, 2020).
URL https://www.meteoblue.com/en/weather/archive/export/basel_switzerland_2661604

[32] W.-Y. He, W.-X. Ren, S. Zhu, Damage detection of beam structures using quasi-static moving load induced displacement response, Engineering Structures 145 (2017) 70–82.

[33] K. Dragomiretskiy, D. Zosso, Variational mode decomposition, IEEE Transactions on Signal Processing 62 (3) (2014) 531–544.

[34] D. Zosso, Variational mode decomposition, matlab central file exchange (Retrieved August 27, 2020).
URL https://www.mathworks.com/matlabcentral/fileexchange/44765-variational-mode-decomposition

[35] Y. Wang, R. Markert, J. Xiang, W. Zheng, Research on variational mode decomposition and its application in detecting rub-impact fault of the rotor system, Mechanical Systems and Signal Processing 60 (2015) 243–251.

[36] D. Kwiatkowski, P. C. Phillips, P. Schmidt, Y. Shin, et al., Testing the null hypothesis of stationarity against the alternative of a unit root, Journal of Econometrics 54 (1-3) (1992) 159–178.

[37] Z. Zhao, W. Chen, X. Wu, P. C. Chen, J. Liu, LSTM network: a deep learning approach for short-term traffic forecast, IET Intelligent Transport Systems 11 (2) (2017) 68–75.

[38] W. Kong, Z. Y. Dong, Y. Jia, D. J. Hill, Y. Xu, Y. Zhang, Short-term residential load forecasting based on LSTM recurrent neural network, IEEE Transactions on Smart Grid 10 (1) (2017) 841–851.

[39] D. P. Kingma, J. Ba, Adam: A method for stochastic optimization, arXiv preprint arXiv:1412.6980 (2014).

[40] Wooden bridge experimental data (Retrieved August 27, 2020).
URL http://users.metropolia.fi/~kullj/JrkwXyZGkhc/

[41] J. Kullaa, Eliminating environmental or operational influences in structural health monitoring using the missing data analysis, Journal of intelligent material systems and structures 20 (11) (2009) 1381–1390.

[42] A. Deraemaeker, A. Preumont, E. Reynders, G. De Roeck, J. Kullaa, V. Lamsa, K. Worden, G. Manson, R. Barthorpe, E. Papatheou, et al., Vibration-based structural health monitoring using large sensor networks, Smart Structures and Systems 6 (3) (2010) 335–347.

[43] J. Kullaa, Distinguishing between sensor fault, structural damage, and environmental or operational effects in structural health monitoring, Mechanical Systems and Signal Processing 25 (8) (2011) 2976–2989.

[44] B. Peeters, System identification and damage detection in civil engeneering (2000).

[45] B. Peeters, G. De Roeck, One-year monitoring of the z24-bridge: environmental effects versus damage events, Earthquake engineering & structural dynamics 30 (2) (2001) 149–171.

[46] E. Reynders, G. Wursten, G. De Roeck, Output-only structural health monitoring in changing environmental conditions by means of nonlinear system identification, Structural Health Monitoring 13 (1) (2014) 82–93.

[47] R. Langone, E. Reynders, S. Mehrkanoon, J. A. Suykens, Automated structural health monitoring based on adaptive kernel spectral clustering, Mechanical Systems and Signal Processing 90 (2017) 64–78.

[48] J. Maeck, G. De Roeck, Description of z24 benchmark, Mechanical Systems and Signal Processing 17 (1) (2003) 127–131.

[49] E. Reynders, G. De Roeck, Vibration-based damage identification: the z24 benchmark (2014).